DEVELOPMENT OF VISCOELASTIC DAMPERS FOR BORING BARS

A THESIS SUBMITTED TO
THE GRADUATE SCHOOL OF NATURAL AND APPLIED SCIENCES
OF
MIDDLE EAST TECHNICAL UNIVERSITY

BY

CIHAT FURKAN KURT

IN PARTIAL FULFILLMENT OF THE REQUIREMENTS
FOR
THE DEGREE OF MASTER OF SCIENCE
IN
MECHANICAL ENGINEERING

DECEMBER 2023

Approval of the thesis:

DEVELOPMENT OF VISCOELASTIC DAMPERS FOR BORING BARS

submitted by **CIHAT FURKAN KURT** in partial fulfillment of the requirements for the degree of **Master of Science in Mechanical Engineering Department, Middle East Technical University** by,

Prof. Dr. Halil Kalıpçılar
Dean, Graduate School of **Natural and Applied Sciences** _______________

Prof. Dr. M. A. Sahir Arıkan
Head of Department, **Mechanical Engineering** _______________

Assist. Prof. Dr. Orkun Özşahin
Supervisor, **Mechanical Engineering, METU** _______________

Assist. Prof. Dr. Gökhan Özgen
Co-supervisor, **Mechanical Engineering, METU** _______________

Examining Committee Members:

Prof. Dr. Ender Ciğeroğlu
Mechanical Engineering, METU _______________

Assist. Prof. Dr. Orkun Özşahin
Mechanical Engineering, METU _______________

Assoc. Prof. Dr. Mehmet Bülent Özer
Mechanical Engineering, METU _______________

Assist. Prof. Dr. Hakan Çalışkan
Mechanical Engineering, METU _______________

Prof. Dr. Erhan Budak
Mechanical Engineering, Sabancı University _______________

Date:

I hereby declare that all information in this document has been obtained and presented in accordance with academic rules and ethical conduct. I also declare that, as required by these rules and conduct, I have fully cited and referenced all material and results that are not original to this work.

Name, Surname: Cihat Furkan Kurt

Signature :

ABSTRACT

DEVELOPMENT OF VISCOELASTIC DAMPERS FOR BORING BARS

Kurt, Cihat Furkan
M.S., Department of Mechanical Engineering
Supervisor: Assist. Prof. Dr. Orkun Özşahin
Co-Supervisor
: Assist. Prof. Dr. Gökhan Özgen

DECEMBER 2023, 89 pages

Self-excited vibrations called chatter is one of the most important problems that occur in machining which causes excessive noise, increased tool wear, poor surface finish, failure of the tool, and/or machine thus reduced productivity. High aspect ratio boring bars with a large Diameter/Length (D/L) ratio exhibit flexibility owing to their geometric characteristics. Consequently, the flexibility in these slender boring bars directly influences the stability of the machining process. To suppress the chatter vibrations, passive or active damping methods can be employed. In this thesis, a novel damping system for slender boring bars is developed using viscoelastic materials. Viscoelastic dampers, integrated into the boring bars using rigid connecting elements, are designed to damp the most flexible mode and prevent chatter vibrations. The effect of the material type, geometry, dimensions, and location of viscoelastic dampers is analyzed using the finite element method. Parameter optimization is achieved by creating design matrices. Finite element analysis demonstrates that the developed dampers effectively reduce the peak amplitudes of flexible modes, resulting in an increase in productivity. Finally, the best design

concept is manufactured and the performance of the designed viscoelastic damper is experimentally verified. The viscoelastic-damped boring bar developed in this study will provide a novel contribution to the literature and directly impact the industry for enhanced productivity.

Keywords: Vibration, Machining, Viscoelastic, Damping, Chatter Suppression

ÖZ

DELİK KATERLERİ İÇİN VİSCOELASTİK SÖNÜMLEYİCİ GELİŞTİRİLMESİ

Kurt, Cihat Furkan
Yüksek Lisans, Makina Mühendisliği Bölümü
Tez Yöneticisi: Dr. Öğr. Üyesi. Orkun Özşahin
Ortak Tez Yöneticisi
: Dr. Öğr. Üyesi. Gökhan Özgen

Aralık 2023 , 89 sayfa

Tırlama ismi verilen kendinden-tahrikli titreşimler; aşırı gürültüye, takım aşınmasının artmasına, kötü yüzey kalitesine, takımın ve/veya makinenin bozulmasına sebep olarak üretkenliğin azalmasına neden olan talaşlı imalat sırasında ortaya çıkan en önemli problemlerden biridir. Ç/U (Çap/Uzunluk) oranı yüksek delik katerleri sahip oldukları geometri sebebiyle esnek takımlardır. Dolayısıyla bu ince delik katerlerindeki esneklik, işlemin kararlılığını doğrudan etkiler. Tırlama titreşimlerini baskılamak için pasif veya aktif sönümleme yöntemleri uygulanabilir. Bu tez çalışmasında ince delik kateri için viskoelastik malzemeler kullanılarak özgün bir sönümleme sistemi geliştirilmiştir. En esnek modu sönümlemek ve tırlama titreşimlerini önlemek amacıyla viskoelastik sönümleyiciler rijit bağlantı parçaları kullanarak delik katerine entegre edilmiştir. Viskoelastik sönümleyicilerin malzeme çeşidi, geometrisi, boyutları ve konumunun etkisi sonlu elemanlar metodu kullanılarak analiz edilmiştir. Tasarım matrisleri oluşturularak parametreler optimuma yaklaştırılmıştır. Geliştirilen sönümleyiciler kullanılarak esnek modların

tepe genliğinin azaltıldığı ve üretkenlikte artış sağlandığı sonlu metodlar analizleri ile gösterilmiştir. Son olarak en iyi konsept tasarım üretilmiş ve viskoelastik damperlerin performansı deneysel olarak doğrulanmıştır. Geliştirilen viskoelastik sönümleyicili boring barın literatüre özgün bir katkısı olacak ve gelişmiş üretkenlik için endüstriye doğrudan etkisi olacaktır.

Anahtar Kelimeler: Titreşim, Talaşlı imalat, Viskoelastik, Sönümleme, Tırlamanın Baskılanması

to my dear family

ACKNOWLEDGMENTS

I would like to express my sincere gratitude to my supervisors, Dr. Orkun Özşahin and Dr. Gökhan Özgen, for their invaluable guidance, unwavering support, and insightful feedback throughout the journey of completing my master's thesis. Their expertise, patience, and dedication have been instrumental in shaping the direction of my research and enhancing the quality of my work.

I am grateful to my family for their unwavering support, patience, and presence during the long and challenging process of writing my thesis. Their confidence and encouragement helped me persevere even in my moments of despair. I attribute my motivation and determination in this study to them.

I would also like to express my gratitude to my close friends from Askalaş group, particularly Mücahit Furkan Yıldız, Ömer Faruk Karakaya and Muammer Tan as well as my friend Semanur Küçük, for their unwavering support, encouragement, and understanding throughout my challenging yet rewarding study. Your belief in me has been a constant source of motivation, and I am truly grateful to have had you by my side.

Finally, I would like to express my gratitude to all my colleagues and friends from Opsin, particularly Arda Akın, Begüm Kavaklıoğlu, Süleyman Yükseldi, Mustafa Gümüş, Oğuz Can Şenel, Emre Yüksel, Gökhan Kulaözü and Ozan Şenyayla for their unwavering support and trust in me. They played a significant role in allowing me to find time for this study in the middle of our busy work schedule. Additionally, I would like to acknowledge Nilgün Bacak, who was not only a colleague but also an excellent study partner during this challenging study process.

I am deeply appreciative of all those who have made significant contributions and provided support throughout my study. Without their guidance and encouragement, this thesis would not have been possible. This important milestone of my academic career would not have been achieved without their involvement.

TABLE OF CONTENTS

ABSTRACT v

ÖZ vii

ACKNOWLEDGMENTS x

TABLE OF CONTENTS xi

LIST OF TABLES xiv

LIST OF FIGURES xvi

LIST OF ABBREVIATIONS xxiv

CHAPTERS

1 INTRODUCTION 1

1.1 Problem Definition 1

1.2 Motivation and Objective of Thesis 1

1.3 Organization of Thesis 2

2 LITERATURE REVIEW 5

2.1 Chatter and Stability 5

2.2 Chatter Vibrations at Boring Bars 6

2.2.1 Passive Solutions 7

2.2.2 Active Solutions 10

3 VISCOELASTIC DAMPERS 13

3.1 Definition of Viscoelastic Dampers 13

3.2 Viscoelastic Materials and Their Modelling 15

3.2.1 Theory and Mathematical Modelling of Viscoelastic Materials 16

3.2.2 Selection of Viscoelastic Material 19

3.2.3 FEM Modelling of a VEM 20

3.3 Conceptual Viscoelastic Damper Designs for Boring Bars 26

3.3.1 Investigation of Conceptual Designs 27

3.3.1.1 Effect of Shear Area of Viscoelastic Dampers 32

3.3.1.2 Effects of Positions of Viscoelastic Dampers 33

3.3.1.3 Effect of VEM Thickness 35

3.3.1.4 Effect of Number of Viscoelastic Dampers 36

3.3.1.5 Position Optimization of Viscoelastic Dampers 38

3.3.1.6 Effect of Dividing The Damper Element 40

3.3.1.7 Effect of Using Dampers of Both Side 43

3.3.1.8 Selection of Best Concepts 44

3.3.2 Optimization of Conceptual Designs 45

4 OPTIMIZATION OF VISCOELASTIC DAMPER PARAMETERS FOR DIFFERENT SCENARIOS 51

4.1 Design Scenarios 52

4.1.1 Scenario 1 - Maximum Damper Diameter Minimum Hole Diameter 53

4.1.2 Scenario 2 - Stepped Boring Bar 53

4.1.3 Scenario 3 - Extra Damper Unit 54

4.2 Optimization of Viscoelastic Dampers for Different Designs Scenarios 54

4.2.1 Optimization for Scenario - 1 54

4.2.2 Optimization for Scenario - 2 56

4.2.3 Optimization for Scenario - 3 60

5 EXPERIMENTAL VALIDATION 65

5.1 Manufacturing of Optimum Design 65

5.2 Experiments 69

5.3 Experimental Results 72

6 RESULTS AND ANALYSIS 75

6.1 Stability Lobe Diagrams 75

6.2 Comparision Against Other Passive Damping Studies 77

7 CONCLUSION 79

REFERENCES 81

APPENDICES

A 87

LIST OF TABLES

TABLES

Table 3.1 Coefficients of 3M ISD - 112 23

Table 3.2 Properties of Verification Beam 24

Table 3.3 Experimental versus FEM Analysis Results 25

Table 3.4 Material Properties of Steel 46

Table 3.5 Peak FRF Amplitudes [mm/N] for CONCEPT-YZ with Different Link Heights and Lengths 46

Table 3.6 Peak FRF Amplitudes [mm/N] for CONCEPT-XZ with Different Link Heights and Lengths 47

Table 3.7 Peak FRF Amplitudes [mm/N] for CONCEPT-YZ with Different VEM Thickness 48

Table 3.8 Peak FRF Amplitudes [mm/N] for CONCEPT-XZ with Different VEM Thickness 48

Table 3.9 Optimized Dampers Performance 50

Table 4.1 Scenario - 1 Performance Comparison 55

Table 4.2 Peak FRF Amplitudes [mm/N] for CONCEPT-YZ with Different Step Diameter and Link Lengths 57

Table 4.3 Peak FRF Amplitudes [mm/N] for CONCEPT-XZ with Different Step Diameter and Link Lengths 57

Table 4.4 Scenario - 2 Performance Comparison 58

Table 4.5 Peak FRF Amplitudes [mm/N] for CONCEPT-XZ with Different Step Diameter and Link Lengths 59

Table 4.6 Scenario - 2 Performance Comparison (40X560) 59

Table 4.7 CONCEPT-YZ Outer Diameter and Link Length Optimization . . . 60

Table 4.8 CONCEPT-XZ Outer Diameter and Link Length Optimization . . . 60

Table 4.9 Peak FRF Amplitudes [mm/N] for CONCEPT-XZ with Different Outer Diameter and Link Length (Connection Diameter=60 mm) 62

Table 4.10 Peak FRF Amplitudes [mm/N] for CONCEPT-XZ with Different Outer Diameter and Link Length (Connection Diameter=70 mm) 62

Table 4.11 Peak FRF Amplitudes [mm/N] for CONCEPT-XZ with Different Outer Diameter and Link Length (Connection Diameter=80 mm) 62

Table 4.12 Scenario - 3 Performance Comparison 63

Table 6.1 Damper Properties of Best Design 77

Table 6.2 Performance of Different Designs 78

LIST OF FIGURES

FIGURES

Figure 2.1 Chip Thickness Variation [1] 6

Figure 2.2 Chip Thickness Variation [1] 7

Figure 2.3 Sandvik Silent Tools Boring Bar [2] 8

Figure 3.1 Bending Configuration 14

Figure 3.2 Tension-Compression Configuration 14

Figure 3.3 Shear Configuration 14

Figure 3.4 Viscoelastic Materials Stress-Strain Versus Time [3] 15

Figure 3.5 Viscoelastic Materials Spring-Dashpot Models [3] 16

Figure 3.6 Variation of The Complex Modulus with Temperature [4] 18

Figure 3.7 Complex Frequency vs. Reduced Frequency [5] 19

Figure 3.8 3M ISD-112 Nomogram [6] 20

Figure 3.9 3M 467 Loss Factor Data at 25 degrees Celsius [7] 20

Figure 3.10 Sample APDL Commands for VEM Modelling 21

Figure 3.11 FEM Model of Reference Damped Beam 24

Figure 3.12 Mesh Details of FEM Model 24

Figure 3.13 Mesh Details of FEM Model 25

Figure 3.14 FRF of Reference Beam 26

Figure 3.15 Solid model of the CONCEPT-BENDING (Target: Bending Deformation of the VEM) 27

Figure 3.16 Solid model of the CONCEPT-TC (Target: Tension-Compression Deformation of the VEM) 27

Figure 3.17 Solid model of the CONCEPT-XY (Target: Shear Deformation of the VEM in XY plane) 28

Figure 3.18 Solid model of the CONCEPT-YZ (Target: Shear Deformation of the VEM in YZ plane) 28

Figure 3.19 Solid model of the CONCEPT-XZ (Target: Shear Deformation of the VEM in XZ plane) 29

Figure 3.20 Solid Model of Bare Boring Bar 29

Figure 3.21 Bare Boring Bar Tip Point FRF 30

Figure 3.22 FEM Model of CONCEPT-XZ 30

Figure 3.23 Mesh Details of CONCEPT-XZ FEM Model 31

Figure 3.24 FRFs of Preliminary Design Concepts 31

Figure 3.25 CONCEPT-YZ with 5mm VEM Height 32

Figure 3.26 CONCEPT-YZ with 12.5mm VEM Height 32

Figure 3.27 CONCEPT-YZ with Different VEM Heights 33

Figure 3.28 Modal Strain Energy for CONCEPT-YZ 33

Figure 3.29 Modal Strain Energy for Viscoelastic Materials for CONCEPT-YZ 34

Figure 3.30 CONCEPT-YZ with 1 Element Near The Fixed End 34

Figure 3.31 FRF Compression of CONCEPT-YZ with 1 and 3 Elements . . . 35

Figure 3.32 FRFs of Single-element CONCEPT-YZ with Different VEM Thicknesses 36

Figure 3.33 CONCEPT-YZ with 3 Parallel DAMPER ELEMENTS 37

Figure 3.34 CONCEPT-XY with 3 Parallel Damper Elements 37

Figure 3.35 CONCEPT-XY with 1 Larger Damper Element 38

Figure 3.36 FRFs of CONCEPT-XY and CONCEPT-YZ with Different Configurations 38

Figure 3.37 Damper Position Parameter X_1 39

Figure 3.38 CONCEPT-YZ with Different Damper Positions 39

Figure 3.39 CONCEPT-XY with Different Damper Positions 40

Figure 3.40 CONCEPT-XY with One Piece Damper 40

Figure 3.41 CONCEPT-XY with Two Pieces Damper 41

Figure 3.42 CONCEPT-XY with One Piece Damper 41

Figure 3.43 CONCEPT-XY with Two Pieces Damper 42

Figure 3.44 FRFs Comparison of One Piece and Two Pieces Dampers 42

Figure 3.45 CONCEPT-YZ Double Sided 43

Figure 3.46 FRFs of CONCEPT-YZ Single and Double Sided 43

Figure 3.47 FRFs of CONCEPT-XY, CONCEPT-YZ and CONCEPT-XZ . . 44

Figure 3.48 FRFs of CONCEPT-XY, CONCEPT-YZ Compared with Bare Bar 45

Figure 3.49 CONCEPT-YZ ∅ = 55mm L = 200mm 47

Figure 3.50 CONCEPT-XZ ∅ = 55mm L = 200mm 48

Figure 3.51 CONCEPT-YZ Double Sided ∅ = 55mm L = 200mm VEMT = 0.24mm 49

Figure 3.52 CONCEPT-XZ Double Sided ∅ = 55mm L = 200mm VEMT = 0.24mm 49

Figure 3.53 FRF Comparison of Optimized Preliminary Designs 50

Figure 4.1 CONCEPT-YZ Double Sided ∅ = 55mm L = 200mm VEMT = 0.24mm 52

Figure 4.2 CONCEPT-XZ Double Sided ∅ = 55mm L = 200mm VEMT = 0.24mm 52

Figure 4.3 Damper Design Scenario - 1 and Design Parameters 53

Figure 4.4 Damper Design Scenario - 2 and Design Parameters 53

Figure 4.5 Damper Design Scenario - 3 and Design Parameters 54

Figure 4.6 Solid Model of CONCEPT-YZ Double Sided Applied to 40 mm Bare Diameter (Best Design of Scenario - 1) 55

Figure 4.7 FRF of Best Design of Scenario - 1 (CONCEPT-YZ Double Sided Applied to 40 mm Bare Diameter) 56

Figure 4.8 FRF of Optimized Designs for Scenario - 2 57

Figure 4.9 50 mm Diameter Boring Bar with Double Sided CONCEPT-XZ Damper Added 40 mm Step 58

Figure 4.10 FRF of Best Design for Scenario - 2 (∅40x560mm Bar) 59

Figure 4.11 FRF of Best Design for Scenario - 3 (∅40x560 mm Bar) 61

Figure 4.12 Double Sided CONCEPT-XZ Damper Added to ∅40x560 mm Bare Bare 61

Figure 4.13 Solid Model of CONCEPT-XZ Double Sided Connection Diameter = 70 mm (Best Design for Scenario - 3) 63

Figure 5.1 Solid Model of Best Design for Scenario - 2 (CONCEPT-XZ Added to 30 mm Step 65

Figure 5.2 Solid Model of Damped Beam with Flat Links 66

Figure 5.3 Manufactured Flat Links 66

Figure 5.4 Manufactured Base Bar 67

Figure 5.5 Manufactured Link Foot 67

Figure 5.6 A Roll of 3M 468MP 67

Figure 5.7 Flat Links with VEM 68

Figure 5.8 Flat Links with VEM 68

Figure 5.9 Damped Bar 68

Figure 5.10 Manufactured Undamped and Damped Bars - 2 69

Figure 5.11 Bare Boring Bar Fixed to Lathe 69

Figure 5.12 Bare Boring Bar Experimentally Obtained FRF 70

Figure 5.13 Bare Boring Bar Simulation Model with Elastic Boundary Condition 70

Figure 5.14 Bare Boring Bar FRFs with Different Loss Factor Values 71

Figure 5.16 Impact Hammer 71

Figure 5.15 Damped Boring Bar Test Setup 72

Figure 5.17 Data Acquisition System 72

Figure 5.18 FRF Results of Experiments and Simulations 73

Figure 6.1 FRF - Real Part 75

Figure 6.2 FRF - İmaginary Part 76

Figure 6.3 SLD of Bare and CONCEPT-XZ Damped Bar 76

Figure 6.4 Best Design 77

LIST OF SYMBOLS

α_T	Shift factor
$\varnothing$	Diameter
γ	Loss Factor
ν	Poisson's ratio
C_1	WLF Constant 1
C_2	WLF Constant 2
$E*$	Complex elastic modulus
E_{imag}	Imaginary part of elastic modulus
E_{real}	Real part of elastic modulus
f	Frequency
$G*$	Complex shear modulus
G_{imag}	Imaginary part of shear modulus
G_{real}	Real part of shear modulus
T	Temperature
T_0	Reference temperature
X_1	Damper Position Parameter

LIST OF ABBREVIATIONS

FRF	Frequency Response Function
FEM	Finite Element Method
VEM	Viscoelastic Material
SLD	Stability Lobe Diagram
FAM	Foamed Aluminum Material
SCDM	SpaceClaim Design Modular
APDL	ANSYS Parametric Design Language
CLD	Constrained Layer Damping
DVA	Dynamic Vibration Absorber
VSDVA	Variable Stiffness Dynamic Vibration Absorber
TMD	Tuned Mass Damper
PID	Particle Impact Damper
MR	Magnetorheological
ER	Electrorheological
CAD	Computer Aided Drawing
WLF	Williams, Landel, and Ferry
SLS	Standard Linear Solid
RKU	Ross, Kerwin and Ungar

CHAPTER 1

INTRODUCTION

1.1 Problem Definition

The realm of machining encompasses a multitude of challenges, and the influence of mechanical vibrations on the process stands out as a critical factor. In operations, especially those involving boring bars, the slender geometries of boring bars lead to a flexible structure. The flexibility induced by this geometry and boundary conditions increases vibration and chatter problems in slender boring bars. The utilization of such slender configurations often presents a conundrum, as their inherent low stability limits necessitate a reduction in the depth of cut. This reduction, in turn, results in a tangible decrease in productivity, unveiling a complex interplay between structural dynamics and machining efficiency.

A primary concern arising from the reduced stability limits is the compromised productivity due to limitations on the depth of cut. This phenomenon not only affects machining speed but also prompts different extra problems. Among these problems are the consequences of vibrations on poor surface quality. Simultaneously, the impact on tool life comes to the forefront, raising concerns about the sustainability and cost-effectiveness of machining operations.

1.2 Motivation and Objective of Thesis

The motivation for this research stems from the inherent challenges presented by the slender geometries of boring bars commonly employed in machining operations. The slender and flexible nature of these structures contributes to an increased susceptibility to vibration and chatter issues, posing significant challenges to machining stability and precision. To address these concerns, numerous studies have explored passive and active design solutions over the years.

This thesis aims to contribute to the ongoing efforts to resolve vibration problems associated with boring bars. In pursuit of this objective, a novel approach is adopted by integrating viscoelastic dampers, a method not previously explored in the context of boring bars and machining applications. The overarching goal is to investigate the effectiveness of viscoelastic dampers in mitigating vibration-related challenges, offering a unique and unexplored avenue for enhancing machining stability. The utilization of viscoelastic dampers is anticipated to introduce a novel and effective solution for chatter problems in boring bars. Through systematic experimentation and analysis, this thesis aims to provide information that contributes to advancing machining technology and alternative boring bar designs.

1.3 Organization of Thesis

This study, aimed at dampening vibrations in boring bars through the use of viscoelastic dampers, will encompass a literature review, the creation of a Finite Element Method (FEM) model for viscoelastic materials using ANSYS, and the generation and optimization of conceptual designs for different usage scenarios. The research will also involve the experimental validation of the analyzed concepts and a comparative analysis of the results with other studies in the literature focusing on boring bar vibration control.

The thesis will be organized into the following key sections to achieve the research objectives:

Chapter - 1 : Introduction

- An overview of the importance of boring bar chatter vibrations is provided.
- The motivation and objectives of the study are stated.
- The scope of the thesis and outline of the structure are stated.

Chapter - 2 : Literature Review

- Chatter and stability are briefly discussed in relation to boring bar vibrations.
- A comprehensive review of existing studies on damping boring bar vibrations available in the literature is conducted.

Chapter - 3 : Viscoelastic Dampers

- The concept of viscoelastic dampers is explained along with a discussion of case studies in which they have been used.
- Viscoelastic materials are defined, and the theoretical background of their modeling is summarized.
- Explanation is provided regarding the selection of the viscoelastic material and the rationale behind its choice.
- The validation of the viscoelastic material model through Harmonic Response analyses using ANSYS Workbench is done.
- Design concepts for integrating viscoelastic dampers into boring bars are presented.
- The created concepts undergo Harmonic Response Analysis, and their vibration control performances are compared.

Chapter - 4 : Optimization of Viscoelastic Damper Parameters for Different Scenarios

- Scenarios of boring bars with viscoelastic dampers are presented.
- The optimization of viscoelastic dampers is carried out for different usage scenarios.

Chapter - 5 : Experimental Validation

- The established experimental setup is described.

- The performance of the dampers is verified by experimentally verifying the analyses performed for the selected concept.

Chapter - 6 : Results and Analysis

- The results obtained from Harmonic Response analyses and simulations of the passive damping systems are presented.
- Stability lobe diagram of most promising result is presented.
- After analyzing the results, the most favorable design is chosen.

Chapter - 7 : Conclusion

- Key findings and achievements of the study are summarized.
- Recommendations for future research are provided.

CHAPTER 2

LITERATURE REVIEW

This chapter provides a brief overview of chatter and stability diagrams in the context of boring bars. The vibrational challenges encountered in boring bars are discussed, outlining the scope of these issues. Subsequently, a comprehensive review of existing literature explores the various studies undertaken to address vibration problems associated with boring bars. The examination of these studies is crucial for understanding the broader landscape of solutions proposed in the literature. The findings from the literature review serve to shed light on the uniqueness and performance of this current study. By assessing the existing body of knowledge, this chapter aims to identify gaps and potential areas for improvement, thereby emphasizing the contributions of the present research in addressing and advancing the understanding of vibration-related issues in boring bars.

2.1 Chatter and Stability

Although CNC tools may seem very rigid, no structure in the real world can be entirely rigid, and they possess a certain degree of flexibility. Due to this flexibility, machining forces cause deformation and vibrations both in tool and the workpiece. This situation leads to variations in the chip thickness throughout the machining process, consequently resulting in fluctuations in machining forces. This gives rise to self-induced vibrations. [1]. Chatter is considered as a self-excited vibration caused by the fluctuating cutting force, resulting in relative vibration between the cutting tool and workpiece [8].

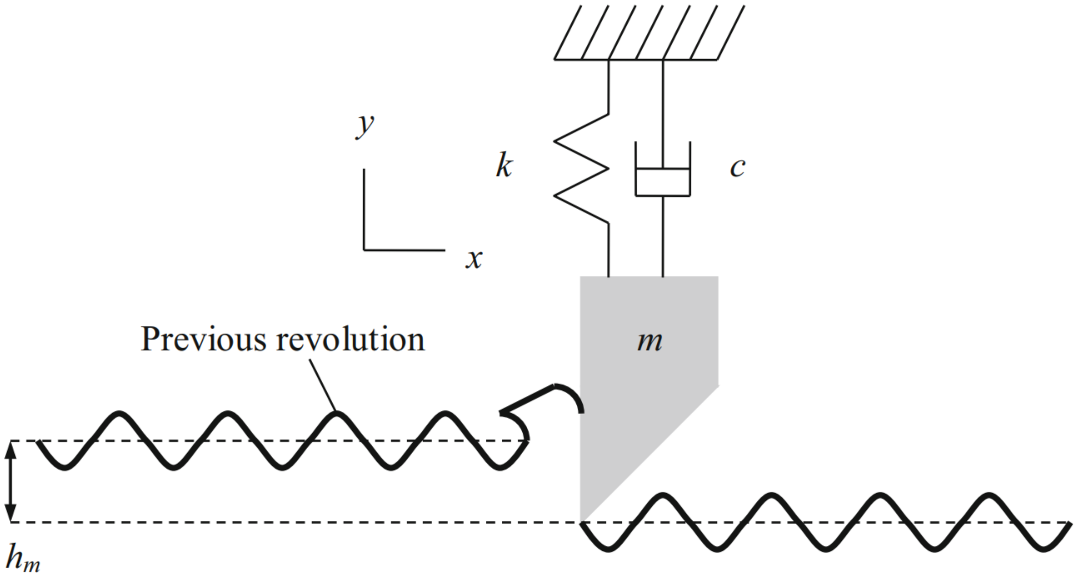

Figure 2.1: Chip Thickness Variation [1]

Stability, on the other hand, refers to the ability of a machining process to maintain a consistent and controlled operation without experiencing chatter. Predicting and ensuring stability is crucial in the field of machining as it directly affects the productivity and quality of the machining process. Stability lobe diagrams (SLDs) are commonly used to determine the chatter-free machining conditions. These diagrams provide spindle speed – axial depth of cut combinations for stable cutting conditions. [9]. An example stability lobe diagram is shown in Figure 2.2.

2.2 Chatter Vibrations at Boring Bars

Chatter vibrations in machining are self-excited vibrations that occur between the tool and the work-piece during the cutting processes. Analytical prediction, experimental study, and vibration analysis techniques are used to predict, identify, and control chatter vibrations in machining. These techniques aim to improve product quality, productivity, and cost-effectiveness in machining operations. Chatter vibrations in boring operations can have a significant impact on the quality of the machined surface and the overall stability of the process. Boring bars, which are commonly used in metal cutting operations, are particularly susceptible to vibrations due to their low inherent stiffness resulting from their high length-to-diameter ratio [10]. As a result, numerous researches have been conducted to damp these vibrations, with the ultimate

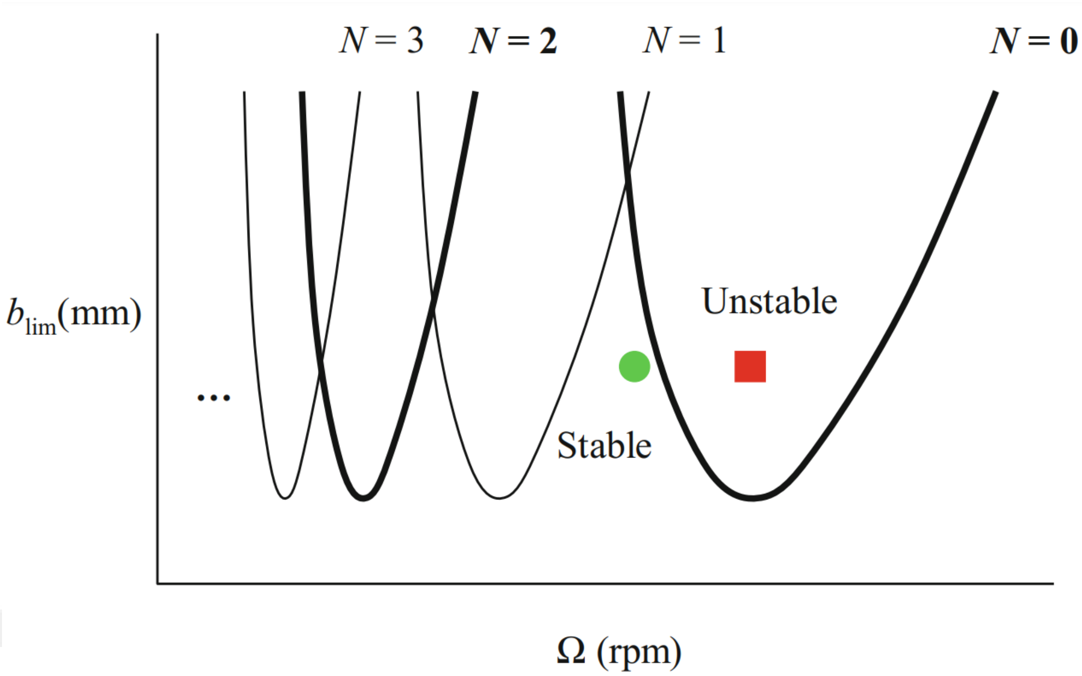

Figure 2.2: Chip Thickness Variation [1]

goal of enhancing surface quality and productivity.

2.2.1 Passive Solutions

In 1984, Takeyama et. al. aimed to achieve improved machining stability through innovative adjustments to the tool holder. The key challenge they addressed was the undesirable vibration known as chatter. Firstly, they opted for a tool holder made from a stiffer material. This choice aimed to enhance the overall rigidity of the setup, thus reducing the propensity for vibration. Secondly, they incorporated a high-damping material into the tool holder. This material effectively absorbed vibrations, diminishing their impact on the machining process. As a result, they observed improvements in the stability diagram [11].

One of the prominent solutions in countering chatter vibrations is the 'Silent Tool' series developed by SANDVIK. This tooling innovation incorporates Tuned Mass Dampers (TMD) within the boring bar, effectively mitigating chatter vibrations. The TMD system is precisely tuned to counteract the frequencies of machining-induced vibrations, leading to smoother and more stable machining operations.

Figure 2.3: Sandvik Silent Tools Boring Bar [2]

One approach to chatter suppression is the use of passive vibration absorbers. Miguélez et. al. studied the behavior of boring bars with passive dynamic vibration absorbers (DVA) and analyzed the stability of a two-degree-of-freedom model [12]. They considered the first mode of vibration of the boring bar and investigated the effects of absorber parameters such as mass, stiffness, damping, and position. In this study, an analytical method is proposed for tuning passive vibration dampers in turning and boring operations.

Another damping study using Tuned Mass Dampers (TMD) was conducted by Liu et. al. in 2016. In this study, the aim was to dampen the vibrations of a boring bar using a structure named as Variable Stiffness Dynamic Vibration Absorber (VSDVA), which allows for adjustable stiffness. Their experimental validation of the approach demonstrated a reduction in vibration amplitudes [13].

Bansal and Law conducted research on the design of a tuned TMD-equipped boring bar using the receptance coupling method. The study yielded improvements in the peak value of the Frequency Response Function (FRF) and the critical stability depth [14]. Zyl et. al. also designed an adaptive tuned mass damper for boring bars. The TMD as a module and can be tuned for different lengths of boring bars. They can achieve seriously huge decrements at the FRF peak point amplitude[15].

Thomas et al. investigate the damping of boring bar vibrations using Particle Impact Damped (PID) and Tuned Mass Damper (TMD) methods. They note that the TMD method provides a greater reduction in the peak FRF value compared to the PID method. Additionally, it is mentioned that the PID method offers a wider range of

L/D values for stable operations compared to the TMD [16].

Chockalingam et al. conducted research on the design of a damped boring bar using the particle damping method. In their study, copper and zinc particles were used individually and in combination in three different scenarios. It was observed that in the scenario where they were used together, improvements in vibration amplitude and surface roughness were achieved [17].

An alternative method used to damp boring bar vibrations is friction. In a study conducted by Hayati et al., pins were press-fitted into channels inside the boring bar to achieve vibration damping through friction. A reduction in the peak real FRF value was observed[18].

Another solution to chatter suppression is using composite boring bars with Constrained Layer Damping (CLD). Yuhuan et al. developed a theoretical analysis model for predicting the chatter stability of composite boring bars with constrained layer damping [19]. They aimed to suppress chatter by improving the damping characteristics of the boring bar.

Studies aiming to achieve vibration damping and stable machining using high-damping materials are also present. Krishna et al. created an implementation of CLD by hollowing out the center of the boring bar and incorporating natural rubber. This approach resulted in observed improvements in surface roughness [20]. Similarly, Song et al. conducted a similar study using a high-damping material called Foamed Aluminum Material (FAM). As a result of their work, they observed enhancements in stability diagrams and surface roughness[21].

In addition to the passive damping techniques mentioned, there are passive damping studies utilizing piezoelectric patches to address boring bar vibrations. Piezoelectric patches can be used both passively and actively. In 2016, Venter et al. studied damping boring bar vibrations using piezoelectric layers in both passive and active modes. They noted that when well-tuned, passive usage can have a similar effect to the active approach [22]. Furthermore, Yiğit et al. aimed to dampen boring bar vibrations and mitigate chatter using the piezoelectric shunt damping method. Their experimental work demonstrated improvements at the absolute stability limit [23].

2.2.2 Active Solutions

In addition to passive solutions, active chatter suppression methods have also been proposed. In 1979, Glaser et. al conducted research to prevent chatter vibrations in boring bars. In this study, two longitudinal channels were created inside the boring bar to form hydraulic chambers. By creating a pressure difference between these two channels, a force was induced at the tool tip. This was an attempt to actively control the vibration of the cutting tool. As a result of the study, a reduction in tool vibration was observed [24].

Tewani et. al conducted a study to reduce vibration in the boring bar by modeling it as a lumped mass system. In this study, instead of a passive Dynamic Vibration Absorber (DVA), an active DVA controlled by piezoelectric actuators was designed and integrated into the boring bar. The Stability Lobe Diagram (SLD) of the systems designed with two different control algorithms was calculated. The results showed that both algorithms in the active solution outperformed the passive approach [25].

Min et al. developed a mechatronic metal cutting tool for precise boring operations. They integrated laser position sensors and piezoelectric actuators into the boring tool body. A control algorithm used for compensation of vibrations of boring bar. Additionally, they integrate a self-monitoring algorithm to detect tool tip failure. The experimental findings indicated enhanced tool precision and dependable detection of process failures [26]. Additionally, various active vibration damping studies using piezoelectric actuators in boring bars can be found in the literature [27] [28] [29].

Wang et. al introduced an innovative design for a tunable-stiffness boring bar that incorporated electrorheological (ER) fluid to tackle chatter during boring. By applying an electric field, they observed significant changes in the bar's stiffness and energy dissipation properties, key to controlling chatter. Wang's research demonstrated that adjusting the electric field within specific ranges related to cutting conditions effectively suppressed chatter during boring, promising improved machining stability and precision [30].

Mei et al. developed a magnetorheological (MR) fluid-controlled boring bar for chatter suppression [31]. Also, Niu et. al. designed a boring bar structure with

MR fluid to suppress chatter vibrations [32].

Another active solution to chatter suppression for a boring bar is using magnetic actuators. Chen et al. developed an active damping system by using magnetic actuators and fiber optic displacement sensors [33].

When examining the presented methods, studies and designs advocating for active vibration control demonstrate commendable performance. However, these approaches involve complexities and costs related to sensors, actuators, and additional power sources, rendering them impractical or scarcely utilized in the market. In addition to active methods, attention has been given to the exploration of various passive techniques to address this issue. Among passive methods, tuned mass dampers are most commonly employed in the market. Nevertheless, these products are both expensive and require precise tuning for optimal performance. Notably, the literature review conducted for this study did not reveal any instances of research employing viscoelastic dampers. The performance of this novel method, to be employed in this thesis, will be systematically compared with the findings presented in existing studies.

CHAPTER 3

VISCOELASTIC DAMPERS

Viscoelastic materials, known for their high-damping properties, have been extensively utilized in various vibration-damping studies. The concept of viscoelastic dampers, predominantly documented in the literature within the field of civil engineering to mitigate vibrations because of earthquake and wind [34], [35], [36], [37], has also been applied by Çağrı Koçan to mitigate vibrations in wind turbine towers [38]. In the context of this thesis, viscoelastic dampers are integrated to boring bars to improve the performance of the tools by decreasing the peak amplitude of the tip point FRFs. This chapter aims to provide a comprehensive overview of the viscoelastic damper concept and conceptual designs pertaining to its integration into boring bars.

3.1 Definition of Viscoelastic Dampers

Viscoelastic damper concepts are employed in vibration-damping studies. The operational principle of these dampers is as follows: rigid links (Grey colored links in Figure 3.1 - Figure 3.3), possessing high energy dissipation properties of viscoelastic materials (Blue colored links in Figure 3.1 - Figure 3.3), connect two points on the structure where vibration damping is desired. These links exhibit relative motion during vibration, leading to deformation within the viscoelastic material and the intentional storage of strain energy. Leveraging the inherent nature of viscoelastic materials, this stored strain energy is subsequently dissipated. The dissipation of this energy, occurring due to the motion, results in the damping of vibrations and reduction of vibration amplitude. Depending on the geometries of how the rigid links are connected with the viscoelastic material, the material is subjected to different deformations. Different damper configurations undergoing bending, tension-compression, and shear deformations are shown in Figure 3.1 - Figure 3.3.

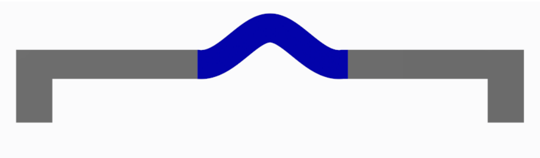

Figure 3.1: Bending Configuration

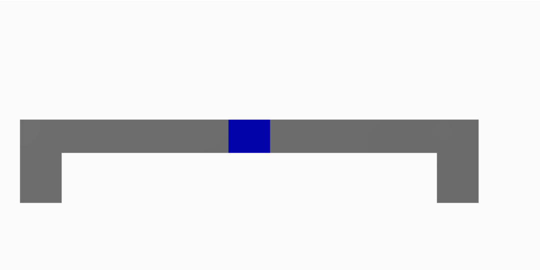

Figure 3.2: Tension-Compression Configuration

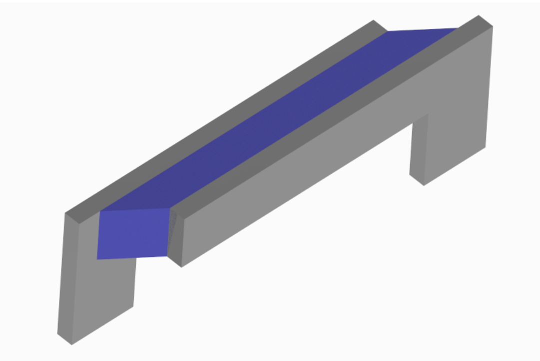

Figure 3.3: Shear Configuration

These different structures of dampers force the viscoelastic material into various deformation modes. The performance of dampers can vary depending on the type of viscoelastic material and its usage. In this study, conceptual designs for different types of viscoelastic materials will be developed to determine the most suitable option

3.2 Viscoelastic Materials and Their Modelling

In this thesis study, the viscoelastic damper concept is used to mitigate vibrations of the boring bar. These dampers have viscoelastic materials as a damping material. Viscoelastic materials behave in both elastic and viscous material properties. The stress-strain relationships change over time (Figure 3.4). Although all materials possess viscoelastic properties, certain materials, such as polymers, biological tissues, and composite materials, exhibit more pronounced viscoelastic behavior [3].

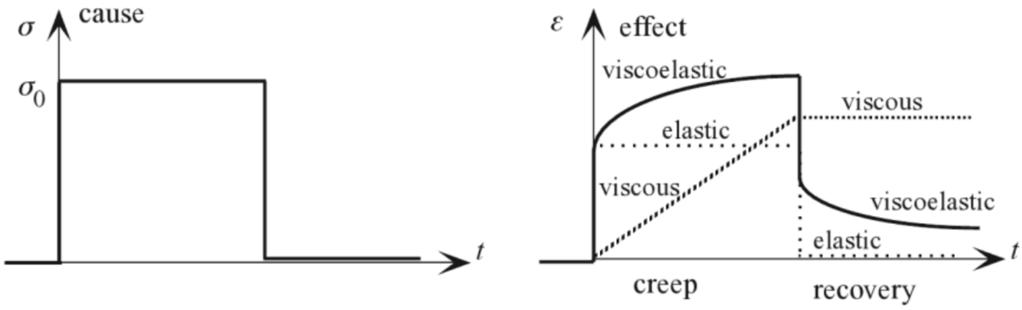

Figure 3.4: Viscoelastic Materials Stress-Strain Versus Time [3]

Viscoelastic materials have a complex elastic modulus, which makes them different from elastic materials. The complex modulus of viscoelastic substances highly varies with frequency and temperature. The complex modulus reflects the viscoelastic behavior of materials. Its dependence on frequency and temperature arises from the dissipation of energy within the material, which affects its mechanical response. Understanding the complex modulus of viscoelastic materials is essential for modeling and predicting their behavior in various applications, such as in the design of structural components. It can be represented as below:

$$E(f)^* = E(f)_{real} + iE(f)_{imag} \tag{3.1}$$

Where E^* represents complex elastic modulus, f is frequency and i is imaginary number. It is the same for shear elastic modulus, where G^* represents complex shear modulus.

$$G(f)^* = G(f)_{real} + iG(f)_{imag} \tag{3.2}$$

3.2.1 Theory and Mathematical Modelling of Viscoelastic Materials

The mathematical modeling of material behaviors and properties is crucial for conducting damping studies and designing structures using viscoelastic materials. Therefore, extensive research has been conducted over the years to develop suitable mathematical models for viscoelastic materials. Linear and non-linear models have been developed. In the context of small stress-strain assumptions as like linear vibration cases like boring bar vibrations, linear viscoelastic modeling has been prominent, allowing for the modeling of behaviors with these simple models. In this section, brief information will be provided about the Maxwell, Kelvin-Voigt, and Standard Linear Solid models. These are the simple models and basis for linear viscoelastic models. Other linear viscoelastic models are created by combining these models. In the books of Lakes and Jones these models are derived, and explanations of these models are represented. [3] [5]. The spring–dashpot models of these models are shown in Figure 3.5. Within Spring-Dashpot models, E denotes the spring stiffness, while η signifies the dashpot viscosity.

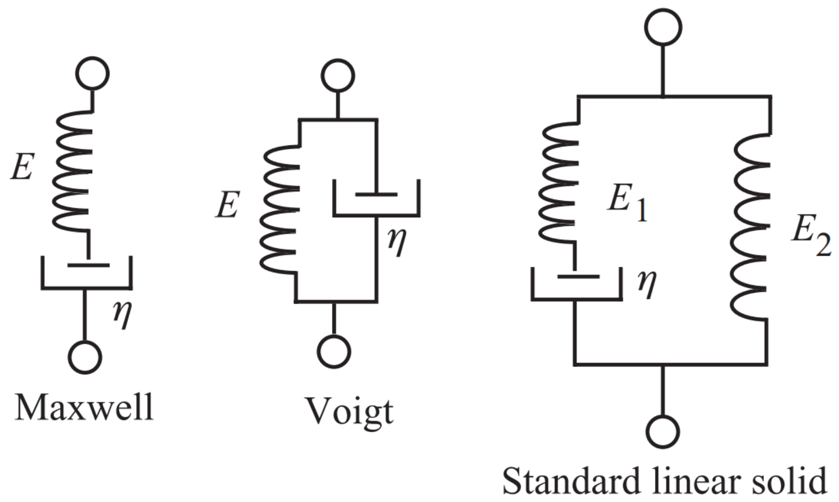

Figure 3.5: Viscoelastic Materials Spring-Dashpot Models [3]

The Maxwell model is composed of a spring and a dashpot arranged in series. Since deformation is considered to be quasi-static, inertia effects are disregarded, resulting in equal force or stress across both elements. The cumulative deformation or strain is the algebraic sum of individual strains[3]. The Equation 3.3 provides the complex modulus [5].

$$E^*(if) = \frac{i2\pi f \nu E}{E + i2\pi f \nu} \tag{3.3}$$

Where ν denotes Poisson's ratio

In contrast, the Kelvin-Voigt model incorporates a spring and a dashpot in parallel, such that both elements experience identical deformation or strain, and the overall stress is the sum of stresses within each component[3]. The Equation 3.4 provides the complex modulus [5].

$$E^*(if) = E + i2\pi f \nu \tag{3.4}$$

The Standard Linear Solid (SLS) model is essentially a Maxwell model augmented by an additional spring element in parallel. This model effectively approximates real material behavior with the exception of its inability to account for variations in storage and loss modulus concerning frequency [3]. The Equation 3.5 provides the complex modulus [5].

$$E^*(if) = \frac{i2\pi f \nu E_1}{E_1 + i2\pi f \nu} + E_2 + i2\pi f \nu \tag{3.5}$$

Where E_1 denotes elastic modulus of spring element in Maxwell part of the model and E_2 is the elastic modulus of additional spring element.

In these models, isothermal conditions are assumed. However, it is important to recognize that the viscoelastic properties of materials can be expected to be influenced by both temperature (T) and frequency (f). This means that the complex modulus function can be represented as $E = E(f, T)$. An illustrative example of the effect of temperature on complex modulus is shown in Figure 3.6.

Considering a material in which viscoelastic behavior arises from processes such as molecular rearrangement or diffusion that occur under stress, the rate of molecular motion determines how fast these processes occur, which is directly related to

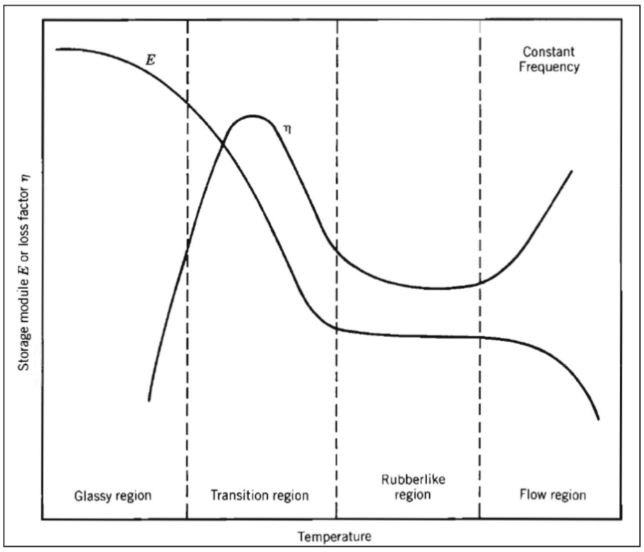

Figure 3.6: Variation of The Complex Modulus with Temperature [4]

temperature. If a temperature increase accelerates all these processes to the same extent, we can express the relaxation function as follows:

$$E(f, T) = E(f\alpha_T(T), T_0) \tag{3.6}$$

Where, $f\alpha_T(T)$ is termed the reduced frequency, T_0 is the reference temperature, and $\alpha_T(T)$ is known as the shift factor. For such materials, a change in temperature effectively stretches or contracts the underlying time scale. Given that viscoelastic properties are typically represented on logarithmic scales of frequency, a change in temperature for such materials corresponds to a horizontal shift of the material property curves along the logarithmic frequency axis. Multiple models exist for the determination of shift factor $\alpha_T(T)$ [5]. Arrhenius and WLF (Williams, Landel, and Ferry) models are presented in Equations 3.7 and 3.8, respectively.

$$\log[\alpha(T)] = T_A \left(\frac{1}{T} - \frac{1}{T_0}\right) \tag{3.7}$$

$$\log[\alpha(T)] = -\frac{C_1(T - T_0)}{C_2 + (T - T_0)} \tag{3.8}$$

Where, T is the operating temperature, C_1 and C_2 represents WLF constants.

At the reference temperature, the complex modulus and loss factor values were determined at various points along the reduced frequency axis. Afterward, these data points were subjected to curve fitting techniques to establish a master curve that effectively encapsulates the viscoelastic material data within the reduced frequency domain. An illustrative example of these reduced frequency curves is shown in Figure 3.7.

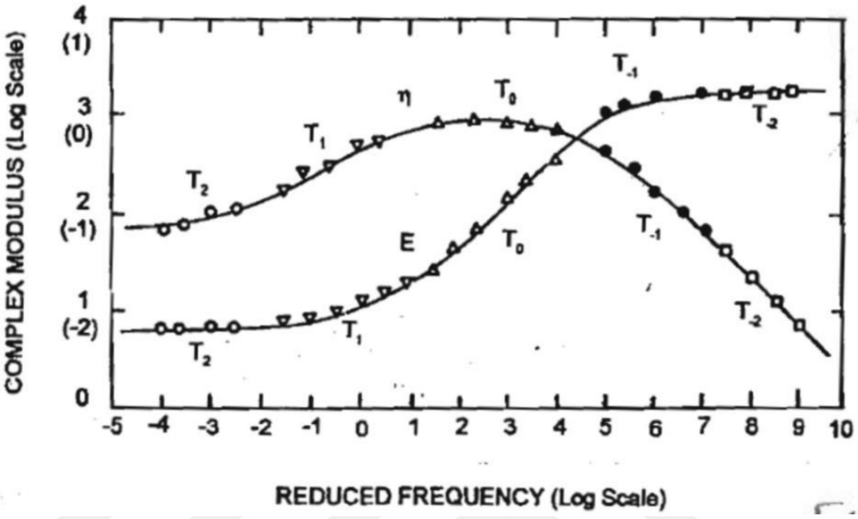

Figure 3.7: Complex Frequency vs. Reduced Frequency [5]

3.2.2 Selection of Viscoelastic Material

The properties of a VEM is changed with temperature. Therefore, to select the appropriate viscoelastic material to use in damping a boring bar, the temperature of a bar in boring operation is investigated. Based on the findings in the literature, it has been observed that while the temperature of the insert increases during the boring process, there is no significant heating on the bar [39][40]. Furthermore, the utilization of damping techniques has been shown to mitigate the temperature rise [40]. Therefore, a viscoelastic material that has good damping properties at room temperature should be used. For that purpose, 3M ISD-112 and 3M 467MP are selected as damping viscoelastic material alternatives in this study. The loss factors of these materials are high at around room temperature. As shown in the nomogram of 3M ISD-112 and experimental loss factor data at 25 degrees Celsius which was taken from 3M Company (Figures 3.8, 3.9). The other reason for the selection of these materials is that they are commercially available products.

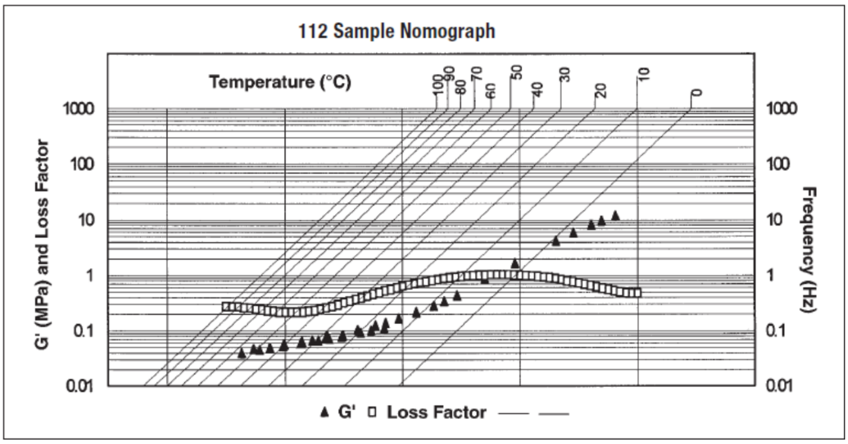

Figure 3.8: 3M ISD-112 Nomogram [6]

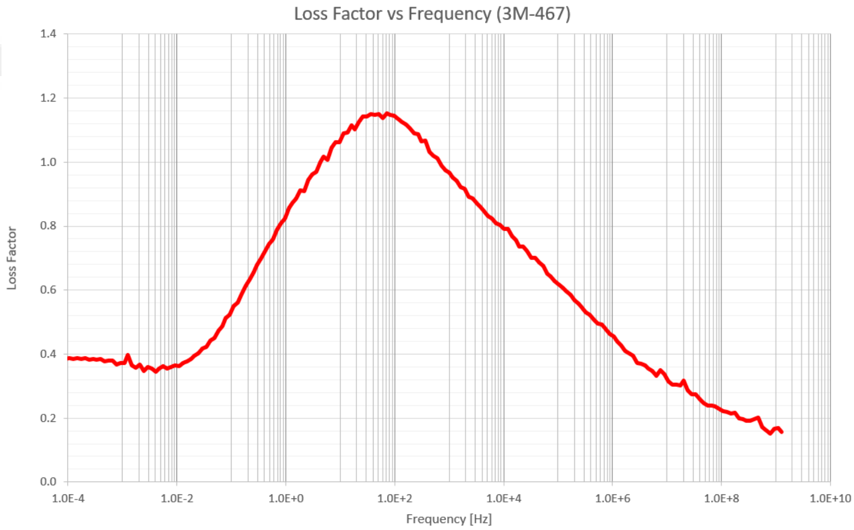

Figure 3.9: 3M 467 Loss Factor Data at 25 degrees Celsius [7]

3.2.3 FEM Modelling of a VEM

The analytical models for viscoelastic materials are not applicable to complex geometries. Therefore, finite element programs such as ANSYS, NASTRAN, ABAQUS are commonly used. In this study, ANSYS Mechanical is used to analyze concept models.

Complex elastic modulus cannot be defined while performing Modal and Harmonic Response analysis in Ansys Workbench software. Therefore, frequency dependent damping effect cannot be simulated by only using Ansys Workbench. To solve that problem, Ansys Parametric Design Language (APDL) codes are written in ANSYS

Workbench model. In the document named "ANSYS Mechanical APDL Material Reference", it is written how viscoelastic material can be modeled in harmonic response analysis using complex elastic modulus [41]. The provided document underscores the adequacy of inputting a set of complex module data and Poisson's ratio data to effectively model a viscoelastic material for a harmonic response analysis [APDL]. For reference and illustration purposes, Figure 3.10 depicts an example APDL command page showcasing the practical implementation of the mentioned modeling approach.

```
Commands
!   Commands inserted into this file will be executed just after material definitions in /PREP7.
!   The material number for this body is equal to the parameter "matid" if it's not a part of a Material Assignment.
!   The element type numbers for this body can be referenced using the 1-D array parameter "typeids".

!   Active UNIT system in Workbench when this object was created:  Metric (mm, kg, N, s, mV, mA)
!   NOTE:  Any data that requires units (such as mass) is assumed to be in the consistent solver unit system.
!                See Solving Units in the help system for more information.

MPDELE,ALL,matid                    ! Deletes all previous material properties
MP,DENS,matid,0.900E-09             ! Density of viscoelastic material
MP,NUXY,matid,0.45                  ! Poisson ratio of viscoelastic material
MP,EX,matid,1                       ! Initial elastic modulus value. (It is not important)

TB,PRONY,matid,,,EXPERIMENTAL       ! Creates empty Prony series table
TB,EXPE,matid,1,,GMODULUS,          ! Creates a table for experimental comples modulus data of viscoelastic material
TBTEMP,288.75                       ! Temperature (It is not important)
TBPT,, 0.00,0.43,0.00,,             ! Frequency dependent experimental complex modulus data
TBPT,, 1.00,0.47,0.07,,
TBPT,, 2.00,0.49,0.11,,
```

Figure 3.10: Sample APDL Commands for VEM Modelling

To create a model as mentioned, an experimental data set for material properties of 3M 467MP is taken from 3M Company. For material properties of 3M ISD–112, there are some material models in the literature [4],[5],[42]. In this study, Soovere's model is used [42]. In Soovere's report, a two-stage standard has been established to reach the complex moduli of viscoelastic materials. In the first stage, to obtain reduced frequency that is used to calculate the complex modulus of a viscoelastic material shift factor α_T is calculated by using Equation 3.9.

$$\log(\alpha_T) = a\left(\frac{1}{T} - \frac{1}{T_Z}\right)^2 + b\left(\frac{1}{T} - \frac{1}{T_Z}\right) + S_{AZ} \tag{3.9}$$

where,

$$C_A = \left(\frac{1}{T_L} - \frac{1}{T_Z}\right)^2 \tag{3.10}$$

$$C_B = \frac{1}{T_L} - \frac{1}{T_Z} \tag{3.11}$$

$$C_C = S_{AL} - S_{AZ} \tag{3.12}$$

$$D_A = \left(\frac{1}{T_H} - \frac{1}{T_Z}\right)^2 \tag{3.13}$$

$$D_B = \frac{1}{T_H} - \frac{1}{T_Z} \tag{3.14}$$

$$D_C = S_{AH} - S_{AZ} \tag{3.15}$$

$$D_E = D_B C_A - C_B D_A \tag{3.16}$$

$$a = \frac{D_B C_C - C_B D_C}{D_E} \tag{3.17}$$

$$a = \frac{C_A D_C - D_A C_C}{D_E} \tag{3.18}$$

Reduced frequency and complex modulus can be calculated as follows (Equation 3.19-3.20).

$$f_R = \alpha_T * f \tag{3.19}$$

$$G^* = \mathrm{G}_{\mathrm{real}} + i\mathrm{G}_{\mathrm{imag}} = (G_e + \frac{G_1}{1 + c_1(\frac{if_R}{f_1})^{-\alpha_1} + (\frac{if_R}{f_1})^{-\beta_1}})MPa \tag{3.20}$$

The necessary coefficients to calculate frequency dependent complex modulus of 3M ISD-112 material are shown in Table 3.1, and the temperature is taken 293.15 Kelvin.

Table 3.1: Coefficients of 3M ISD - 112

Coefficient	Value
T_Z	290
T_L	210
T_H	360
S_{AZ}	0.05956
S_{AL}	0.1474
S_{AH}	0.009725
G_e	0.4307
G_1	1200
f_1	1.54E+06
β_1	0.6847
c_1	3.241
α_1	0.18

A MATLAB script has been developed to derive frequency-dependent material properties for the ISD-112 material. Employing the specified equations and coefficients, this script is designed to compute and present these material properties in the APDL format. The codes given in the appendix section.

In addition to modeling material properties, a decision was made to employ either SOLID185 or SOLID186 element types, along with the "Shared Topology" approach, utilizing the SCDM software. This choice was informed by the research conducted by Çavuş in his master's thesis, where he thoroughly investigated and recommended the appropriate meshing and contact type selections [43].

In order to establish the credibility and accuracy of the proposed model, a validation process was conducted using a cantilever beam. The relevant properties (Table 3.2 and corresponding experimental results of this cantilever beam were sourced from the master's thesis authored by Eyyuboglu [44].

Since the boundary condition on the fixed side could not be fully met in the experimental setup, a 151.7 mm long beam was modeled in the FEM model as

Table 3.2: Properties of Verification Beam

Parameter	Value	Units
Beam Length	150	mm
Beam Width	12.7	mm
Base Layer Thickness	3.15	mm
Base Layer Material	ALUMINUM 6061	N/A
Base Layer Material Density	2700	kg/m^3
Base Layer Material Elastic Modulus	68.9	GPa
Base Layer Material Poisson's Ratio	0.33	N/A
Damping Layer Thickness	0.127	mm
Damping Layer Material	3M ISD-112	N/A
Damping Layer Material Density	900	kg/m^3
Damping Layer Material Elastic Modulus	FREQ. DEP.	N/A
Damping Layer Material Poisson's Ratio	0.45	N/A
Constraining Layer Thickness	0.254	mm
Constraining Layer Material	ALUMINUM	N/A
Constraining Layer Material Density	2700	kg/m^3
Constraining Layer Material Elastic Modulus	70	GPa
Constraining Layer Material Poisson's Ratio	0.33	N/A

calculated in the thesis. A structural damping of 0.006 is entered for the aluminum material. In addition, 0.25 gr point mass is given to the endpoint to reflect the effect of the accelerometer and cable weights on the simulation. In FEM model 1020 SOLID186 elements are used, and it is represented in Figure 3.11, Figure 3.12 and Figure 3.13. A comparison of the obtained results is given in Table 3.3.

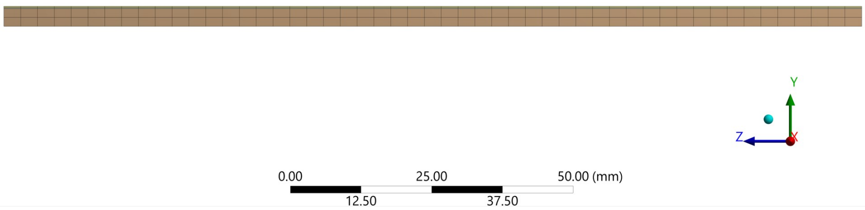

Figure 3.11: FEM Model of Reference Damped Beam

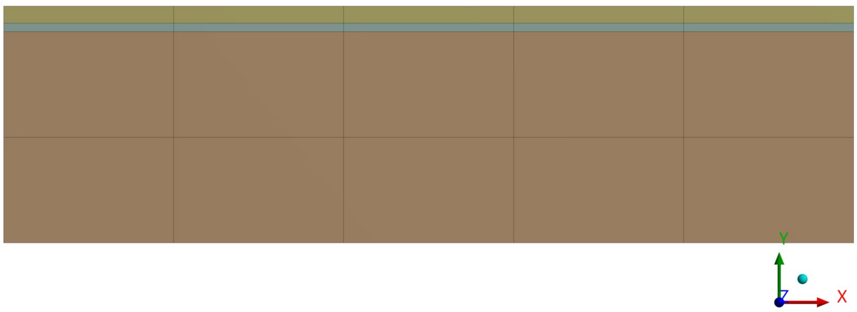

Figure 3.12: Mesh Details of FEM Model

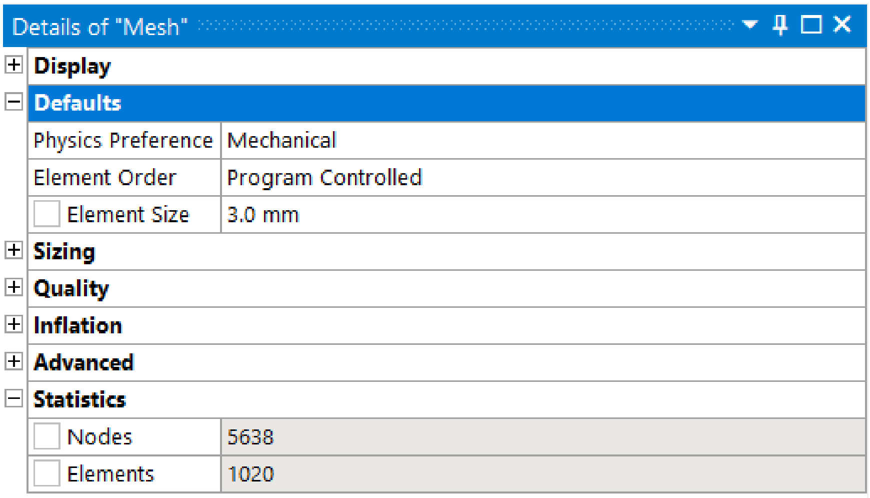

Figure 3.13: Mesh Details of FEM Model

Table 3.3: Experimental versus FEM Analysis Results

	Natural Frequency [Hz]		**% Error**
Mode	**Experimental**	**FEM**	
First	118.5	118	0.421941
Second	737	729	1.085482
Third	2052.3	2032	0.989134

Evident from the natural frequency outcomes, it becomes apparent that the FEM simulation yields highly accurate results. The findings indicate a robust correlation between the predicted natural frequencies and the corresponding experimental measurements. Jones represents the Ross, Kerwin and Ungar (RKU) method to analyze the effects of viscoelastic material damping on the vibration behavior of simple structures like beams [5]. The RKU method is based on a three-layered beam model, and is proper for using CLD systems. The method assumes pure sinusoidal mode shapes and has been used in many analytical works. The method provides proper accuracy. Therefore, after validation of the FEM model with experimental natural frequency findings, by removing the added point mass, the analysis was run again, and the results were compared with the analytical solution of the same beam which is obtained by using RKU equations. (Figure 3.14. The results show that the model is highly accurate.

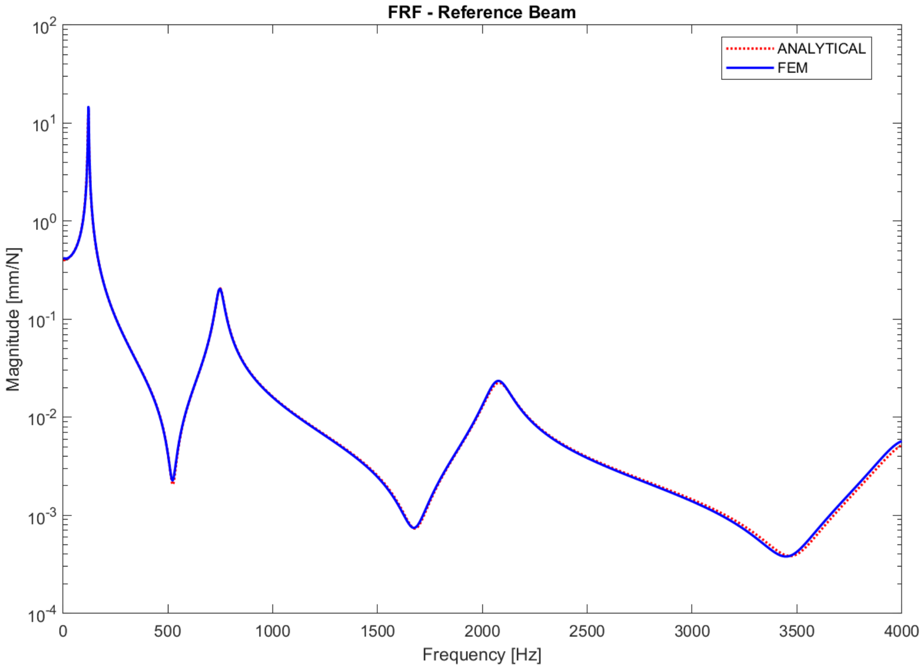

Figure 3.14: FRF of Reference Beam

The obtained results demonstrate that the proposed model achieves a remarkable level of accuracy when compared to both the analytical solution and experimental studies. Therefore, the same method was used to model VEM in the analysis of concept designs in this study.

3.3 Conceptual Viscoelastic Damper Designs for Boring Bars

The different viscoelastic damper configurations described were planned to be integrated into the boring bar, and concept designs were created. One of these concepts, denominated as CONCEPT-BENDING and visually depicted in Figure 3.15, is primarily designed to achieve damping by subjecting the viscoelastic material to bending deformations. Another concept, denoted as CONCEPT-TC and presented in Figure 3.16, is designed to provide damping through the imposition of tension-compression deformations on the viscoelastic material. In Figure 3.17, the concept CONCEPT-XY is introduced, characterized by its aim to deliver damping by subjecting the viscoelastic material to shear deformations specifically within the

XY plane. Then, in Figure 3.18, the concept CONCEPT-YZ is featured, emphasizing its purpose to realize damping by imposing shear deformations on the viscoelastic material, this time within the YZ plane. Finally, in Figure 3.19, the concept CONCEPT-XZ is presented. The goal is to subject the viscoelastic material to shear deformations specifically within the XZ plane.

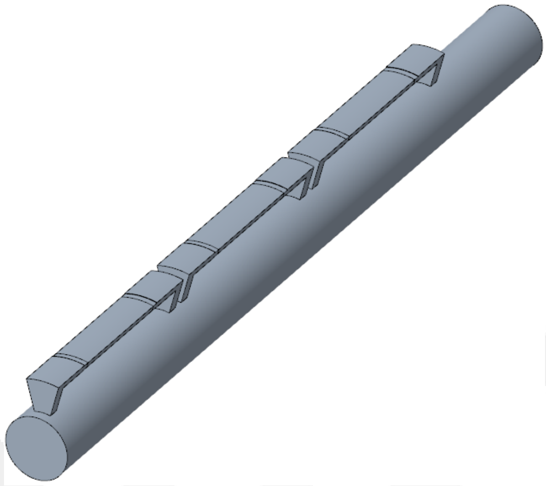

Figure 3.15: Solid model of the CONCEPT-BENDING (Target: Bending Deformation of the VEM)

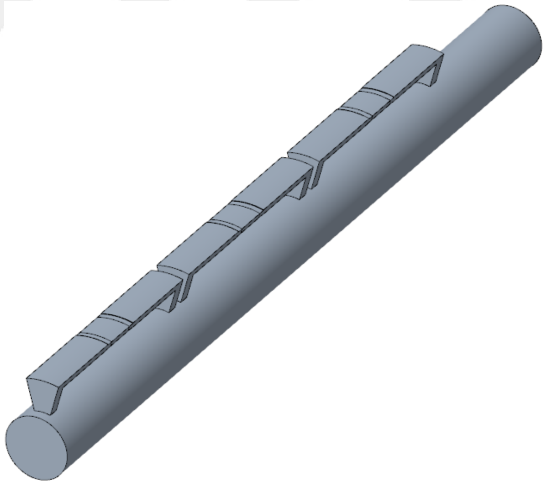

Figure 3.16: Solid model of the CONCEPT-TC (Target: Tension-Compression Deformation of the VEM)

3.3.1 Investigation of Conceptual Designs

Higher Length/Diameter (L/D) ratio in boring bars increases their flexibility and makes them more prone to chatter vibrations.Therefore boring bar with an L/D ratio

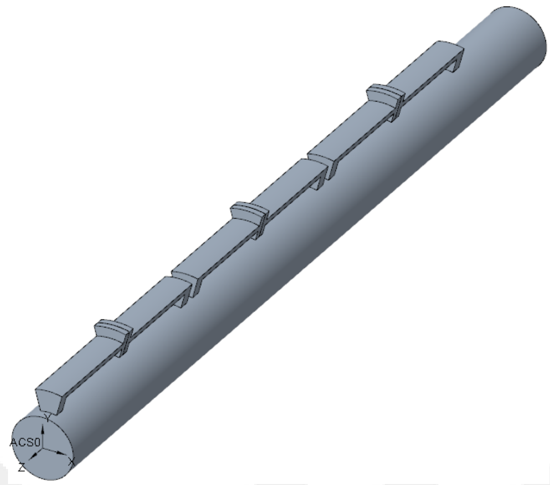

Figure 3.17: Solid model of the CONCEPT-XY (Target: Shear Deformation of the VEM in XY plane)

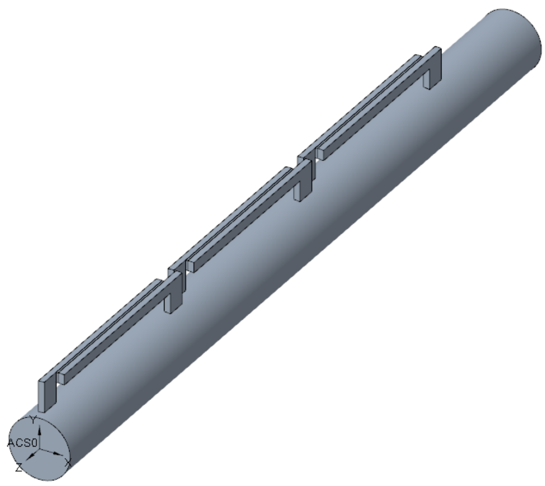

Figure 3.18: Solid model of the CONCEPT-YZ (Target: Shear Deformation of the VEM in YZ plane)

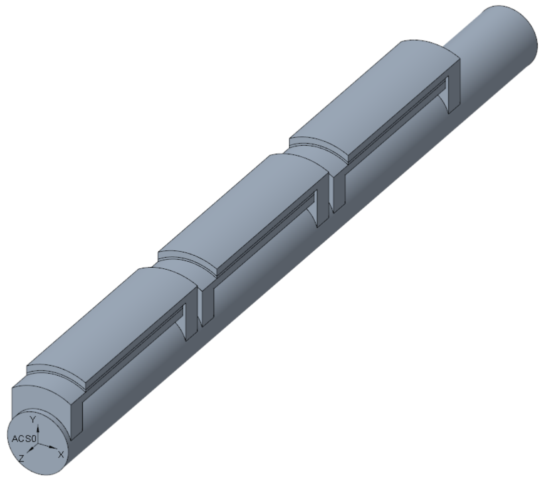

Figure 3.19: Solid model of the CONCEPT-XZ (Target: Shear Deformation of the VEM in XZ plane)

greater than 10 (400 mm length and 30 mm diameter) has been chosen as the base model (Figure 3.20). Consequently, a cylinder with a diameter of 30 mm and a length of 400 mm has been selected as the boring bar model (Figure 3.20). Designed viscoelastic dampers are added to that bar and tip point FRFs will be calculated. Bare bar FRFs will be used to evaluate the performance of the proposed design and will be taken as a reference.

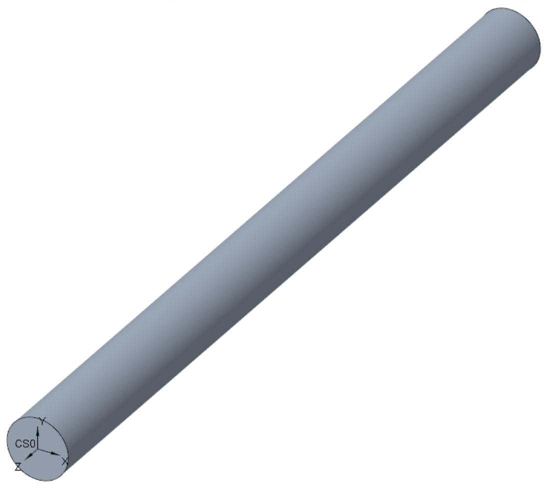

Figure 3.20: Solid Model of Bare Boring Bar

To identify the most flexible mode of the bare boring bar that viscoelastic dampers will be applied, and to determine the frequency range for subsequent analyses, a Harmonic Response Analysis was conducted using ANSYS Mechanical. The tip point FRF graph, as shown in Figure 3.21, was obtained. As expected for a cantilever beam like the boring bar, the results clearly indicate that the first mode is the most flexible and dominant.

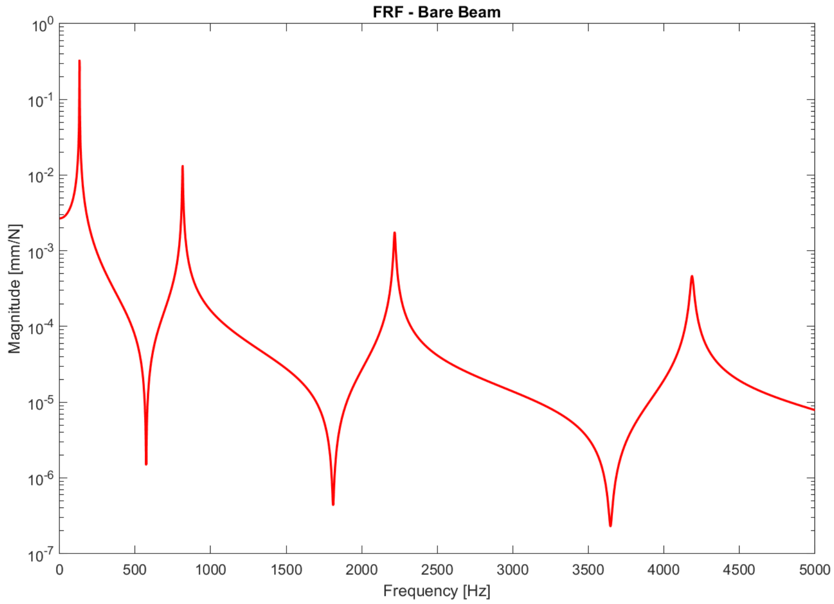

Figure 3.21: Bare Boring Bar Tip Point FRF

In order to evaluate the impacts of these five damper configurations, preliminary concept designs were subjected to FEM analysis. To serve as an example for FEM models, the model and mesh details of the CONCEPT-XZ design are presented in Figure 3.22 and Figure 3.23. As previously validated, the SOLID186 element type was employed during the VEM modeling process.

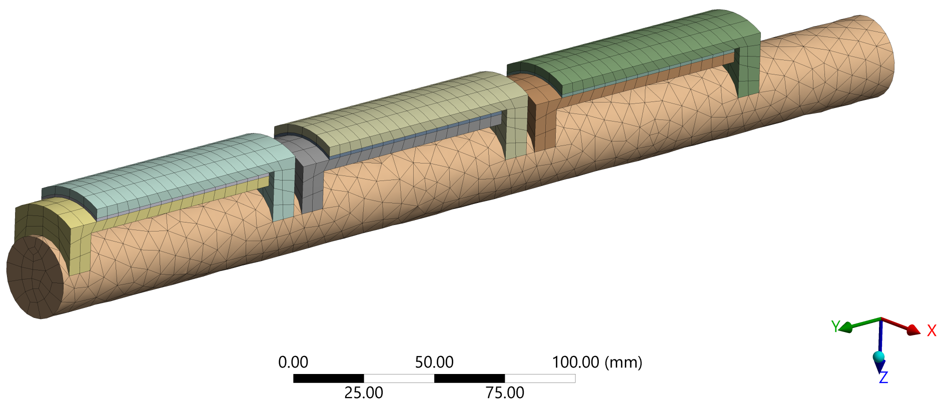

Figure 3.22: FEM Model of CONCEPT-XZ

Then, tip point FRFs are calculated using the harmonic analysis in ANSYS, and

Display	
Display Style	Use Geometry Setting
Defaults	
Physics Preference	Mechanical
Element Order	Quadratic
Element Size	7.5 mm
Sizing	
Quality	
Inflation	
Advanced	
Statistics	
Nodes	12819
Elements	3859

```
*** ELEMENT MATRIX FORMULATION TIMES
  TYPE    NUMBER   ENAME      TOTAL CP  AVE CP

     1     1089  SOLID187      0.250   0.000230
     2     1990  SOLID186      0.953   0.000479
     3      108  SOLID186      0.062   0.000579
     4       88  SOLID186      0.047   0.000533
     5       64  SOLID186      0.031   0.000488
     6      108  SOLID186      0.047   0.000434
     7       88  SOLID186      0.078   0.000888
     8       64  SOLID186      0.047   0.000732
     9      108  SOLID186      0.031   0.000289
    10       88  SOLID186      0.031   0.000355
    11       64  SOLID186      0.031   0.000488
    12       27  SURF154       0.000   0.000000
Time at end of element matrix formulation CP = 4.1875.
```

Figure 3.23: Mesh Details of CONCEPT-XZ FEM Model

obtained results for the proposed designs are given in Figure 3.24 along with the bare bar FRF. As seen from the result, the peak amplitude of the flexible mode decreases by implementing the designed dampers. Also, the FRF results have indicated that the CONCEPT-XY, CONCEPT-YZ and CONCEPT-XZ configurations exhibit higher effectiveness. Consequently, the design development stages will proceed with these three concept designs.

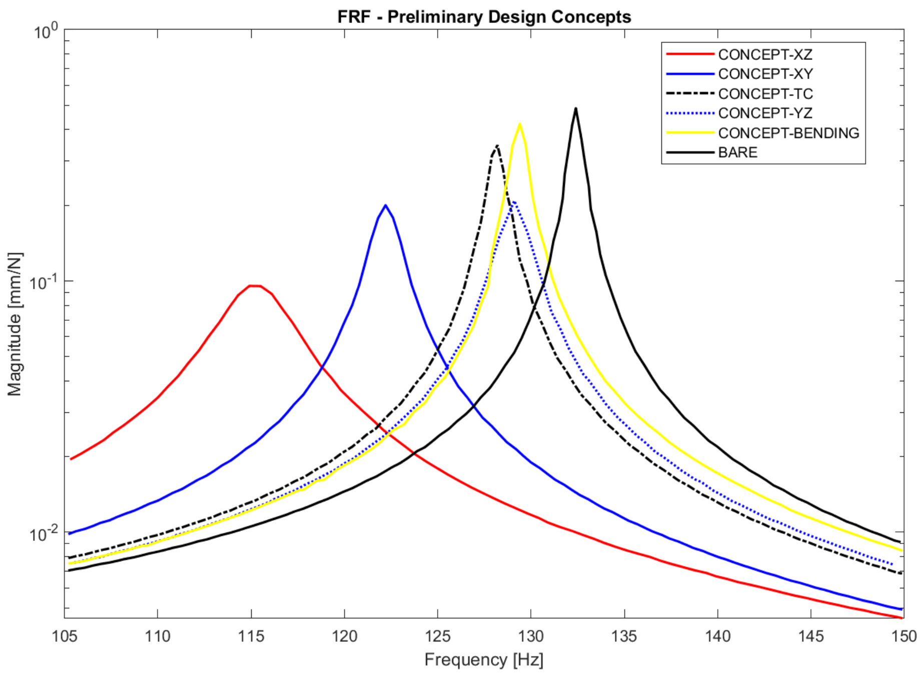

Figure 3.24: FRFs of Preliminary Design Concepts

3.3.1.1 Effect of Shear Area of Viscoelastic Dampers

To investigate the effect of shear area, CONCEPT-YZ is analyzed by changing the VEM height. The subsequent step involved an increase in the height of the links in the CONCEPT-YZ configuration while keeping the maximum outer diameter constant to observe the effect of the shear area on performance (Figure 3.25, Figure 3.26).In both concepts, a VEM thickness of 1mm was utilized. The FRF results are presented in Figure 3.27.

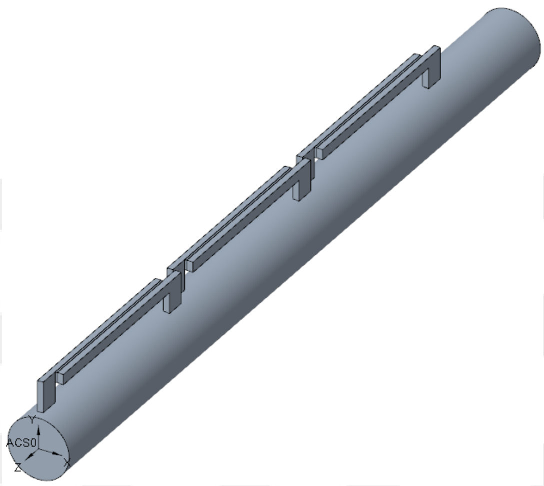

Figure 3.25: CONCEPT-YZ with 5mm VEM Height

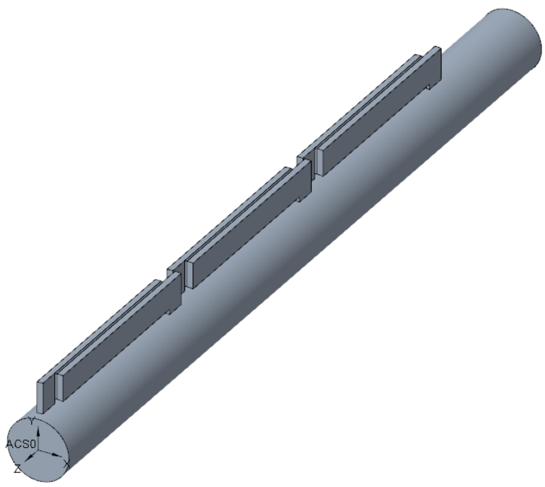

Figure 3.26: CONCEPT-YZ with 12.5mm VEM Height

As shown in Figure 3.26, VEM height directly effects the performance. For the analyzed case, increasing the VEM height to 12.5 mm, peak amplitude decreases 1.64 times compared to 5 mm VEM height. Since the results demonstrated a positive effect of enlarging the shear area, the enlarged shear area links will be utilized for

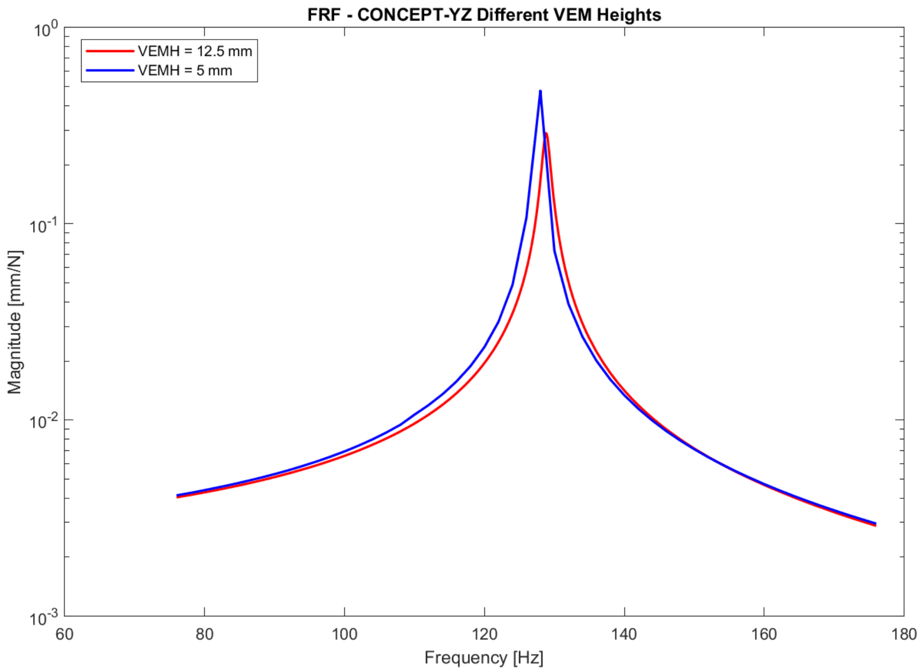

Figure 3.27: CONCEPT-YZ with Different VEM Heights

further progression.

3.3.1.2 Effects of Positions of Viscoelastic Dampers

To analyze the effect of the viscoelastic damper positions on the boring bar, the modal strain energies of CONCEPT-XY for the specific mode are calculated using ANSYS Mechanical, and obtained results are shown in Figure 3.28 and Figure 3.29. As seen from Figure 3.28 and Figure 3.29, it becomes apparent that there is minimal accumulation of strain energy within the VEM layers near the free end, whereas it predominantly accumulates near the fixed end of the bar.

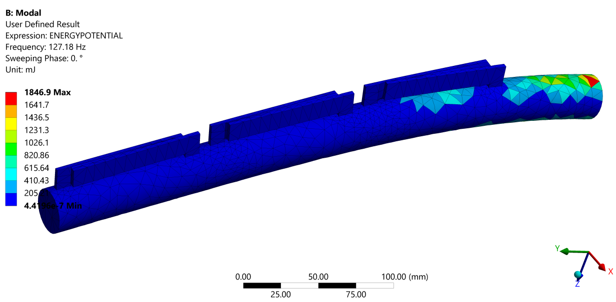

Figure 3.28: Modal Strain Energy for CONCEPT-YZ

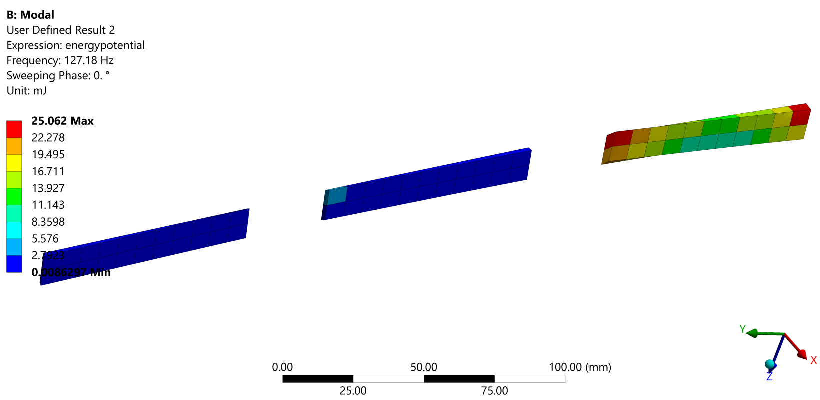

Figure 3.29: Modal Strain Energy for Viscoelastic Materials for CONCEPT-YZ

After analyzing the data displayed in Figure 3.28 and Figure 3.29, it was determined that the initial design required modifications for optimal performance. The recommended design adjustment involved removing two rigid links situated near the free end as depicted in Figure 3.30. Through the use of Harmonic Response analysis, the frequency response functions (FRFs) for both the three-element and single-element CONCEPT-YZ designs were computed. The resulting FRFs are displayed in Figure 3.31, providing a clear comparison of the performance of each design.

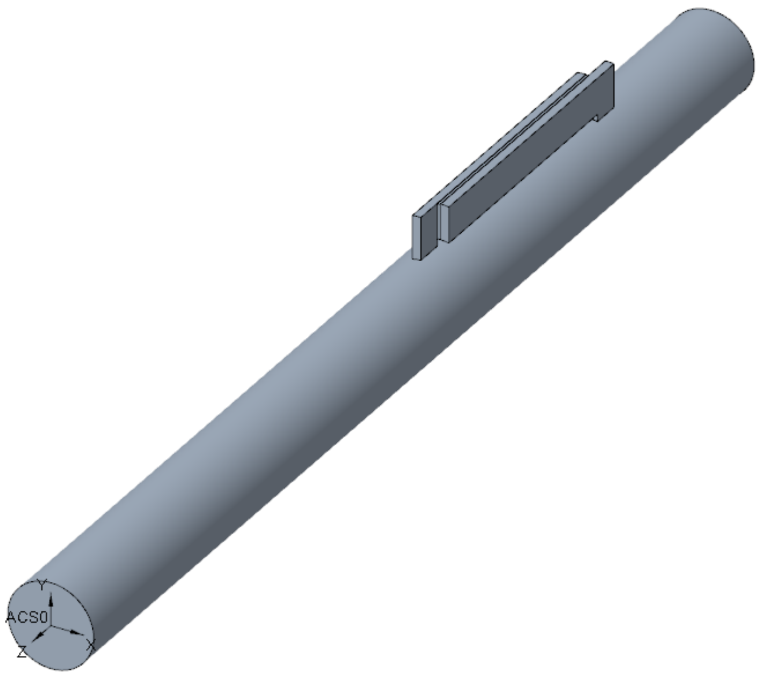

Figure 3.30: CONCEPT-YZ with 1 Element Near The Fixed End

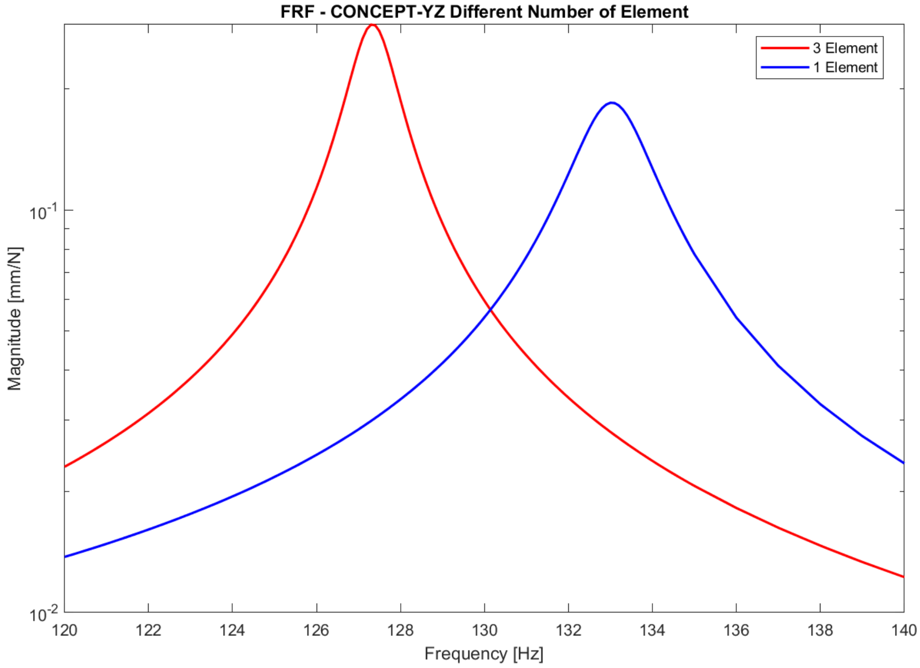

Figure 3.31: FRF Compression of CONCEPT-YZ with 1 and 3 Elements

A thorough analysis of the results revealed that the removal of the damper elements at the free end has led to an increase in the resonance frequency, although it was not independently sufficient, and has simultaneously resulted in a decrease in amplitude. As seen from Figure 3.31, using a single element provides better performance and for the analyzed case, 1 VEM element provides 36% lower peak amplitude compared to 3 VEM elements.

Upon examining the results, it was observed that the removal of links near the free end increased the resonance frequency and led to a decrease in amplitude, although it was not sufficient on its own. As indicated by these findings, in future concept studies, damping links will be positioned closer to the fixed end.

3.3.1.3 Effect of VEM Thickness

To investigate the impact of VEM thickness on performance, the single-element CONCEPT-YZ configuration was analyzed with VEM thicknesses of 1mm, 0.75mm, 0.5mm, 0.3mm, and 0.15mm. Free-end FRFs were computed with various VEM thicknesses, as shown in Figure 3.32.

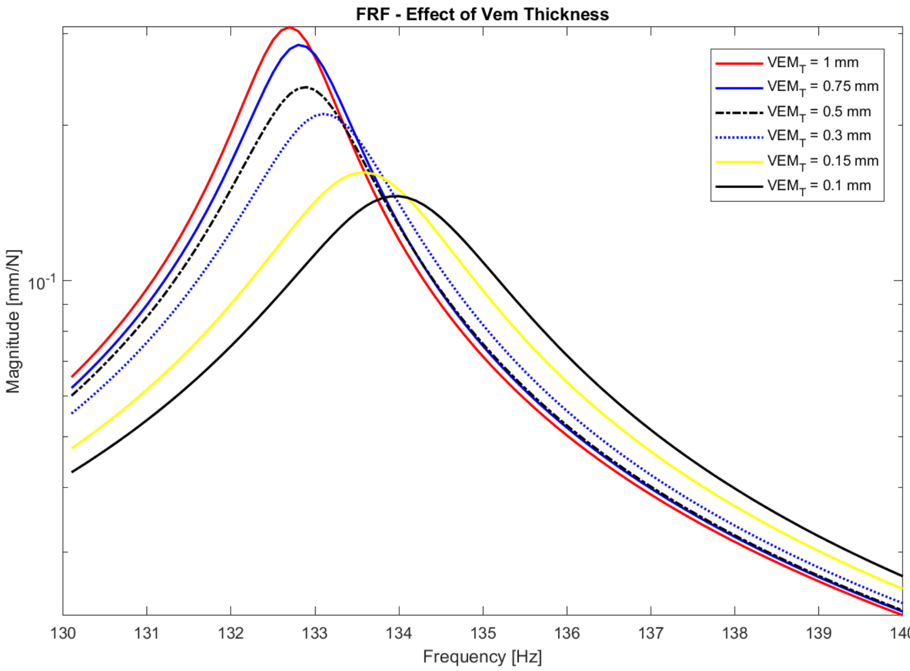

Figure 3.32: FRFs of Single-element CONCEPT-YZ with Different VEM Thicknesses

As seen from Figure 3.32, VEM thickness directly affects performance. It seems there is an inverse proportion between VEM thickness and damping performance. However, it could be different for different concepts and materials. Therefore, for forthcoming design optimization phases, VEM thickness emerges as a pivotal parameter that demands careful consideration. It will be among the integral factors to be fine-tuned and optimized in pursuit of achieving the highest level of damping performance and efficiency in the system.

3.3.1.4 Effect of Number of Viscoelastic Dampers

Until this stage, viscoelastic dampers in both the CONCEPT-YZ and CONCEPT-XY configurations have been exclusively positioned at the center. To further explore the design space, three-element designs were created for both concepts by adding dampers of the same axial position and dimensions adjacent to the central dampers. These designs are visually represented in Figure 3.33 and Figure 3.34.

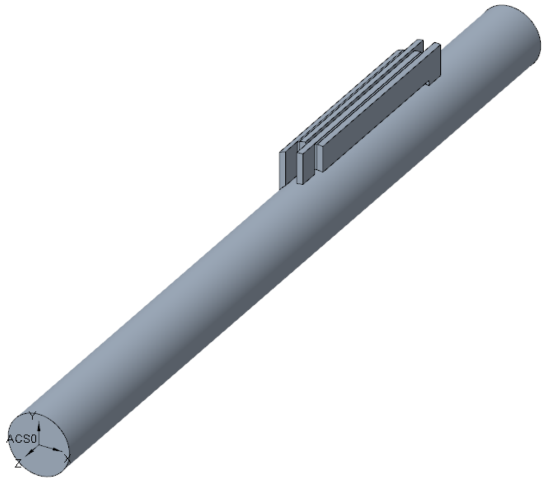

Figure 3.33: CONCEPT-YZ with 3 Parallel DAMPER ELEMENTS

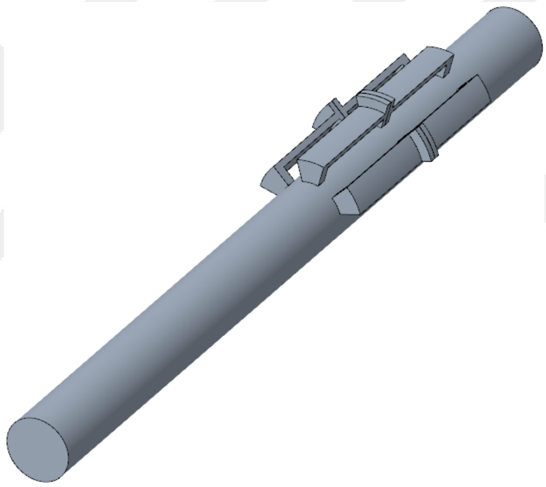

Figure 3.34: CONCEPT-XY with 3 Parallel Damper Elements

Additionally, an alternative design was introduced for the CONCEPT-XY configuration, featuring a single large damper structure covering the same area as the three damper elements. This design is visually presented in Figure 3.35

Harmonic response analyses were conducted for these four designs, and the results are presented in Figure 3.36. The FRF results indicate that the three-element parallel damper structure in the CONCEPT-YZ and the single large damper structure in the CONCEPT-XY configurations provide higher levels of damping. Furthermore, these two designs exhibit closely matched performance results.

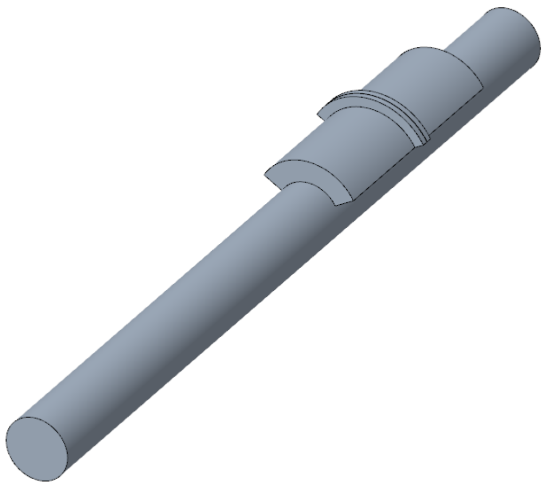

Figure 3.35: CONCEPT-XY with 1 Larger Damper Element

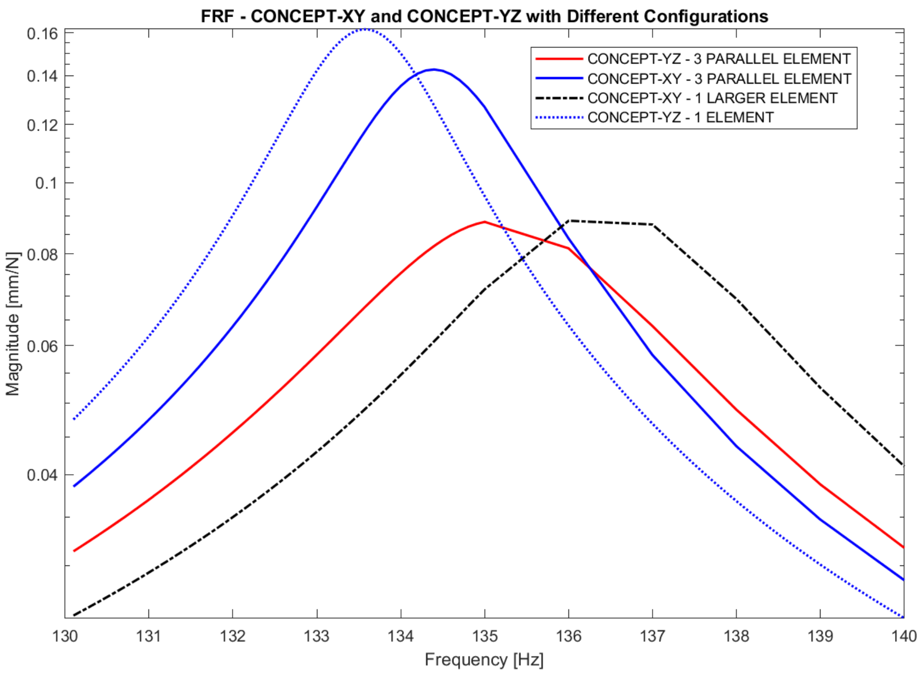

Figure 3.36: FRFs of CONCEPT-XY and CONCEPT-YZ with Different Configurations

3.3.1.5 Position Optimization of Viscoelastic Dampers

Previous analyses showed that having the dampers close to the fixed end yields better performance. To determine the optimal damper position, designs were created by altering the X_1 parameter, as shown in Figure 3.37. In these designs, the outer diameter, link length, and VEM thickness remained constant, with only the positions of the dampers being adjusted by varying the X_1 parameter.

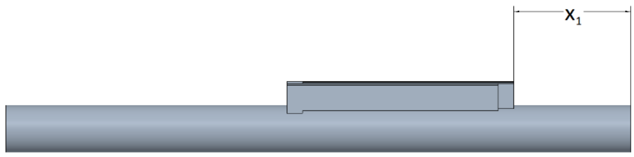

Figure 3.37: Damper Position Parameter X_1

Optimization of link positions was conducted for both the CONCEPT-YZ and CONCEPT-XY configurations. Harmonic Response Analysis was executed for different link positions for both concepts, resulting in the computation of free-end FRFs. These calculated FRFs are presented comparatively in Figure 3.38 and Figure 3.39. It was observed that performance improved as the dampers were moved closer to the fixed end for both concepts. To ensure that the attachment and movements of the boring bar would not pose any issues, the dampers were positioned 5mm away from the nearest fixed end. As a result of these findings, it was decided that in the subsequent designs, the dampers would be located 5mm away from the fixed end.

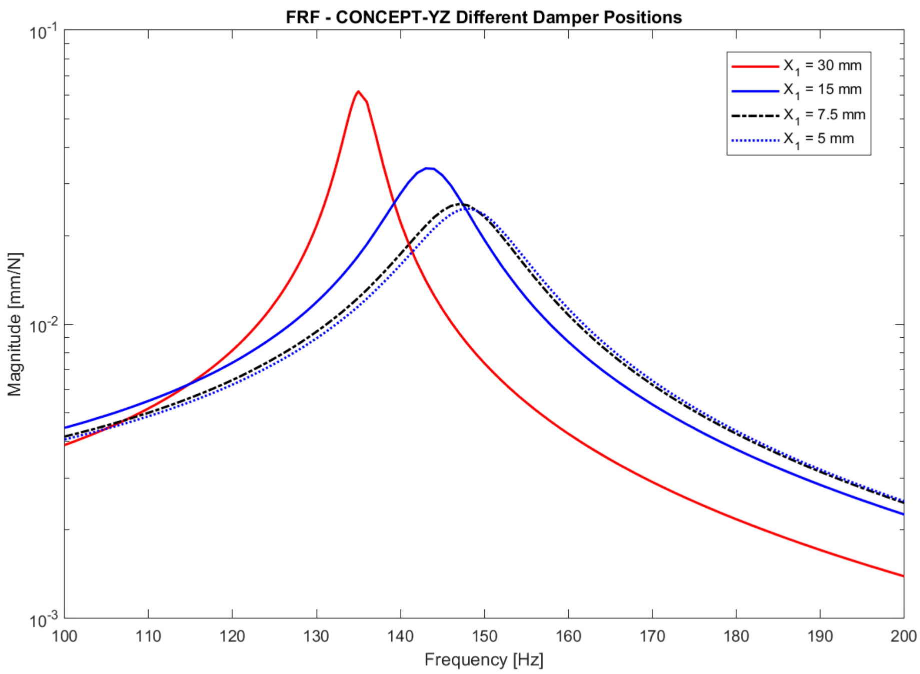

Figure 3.38: CONCEPT-YZ with Different Damper Positions

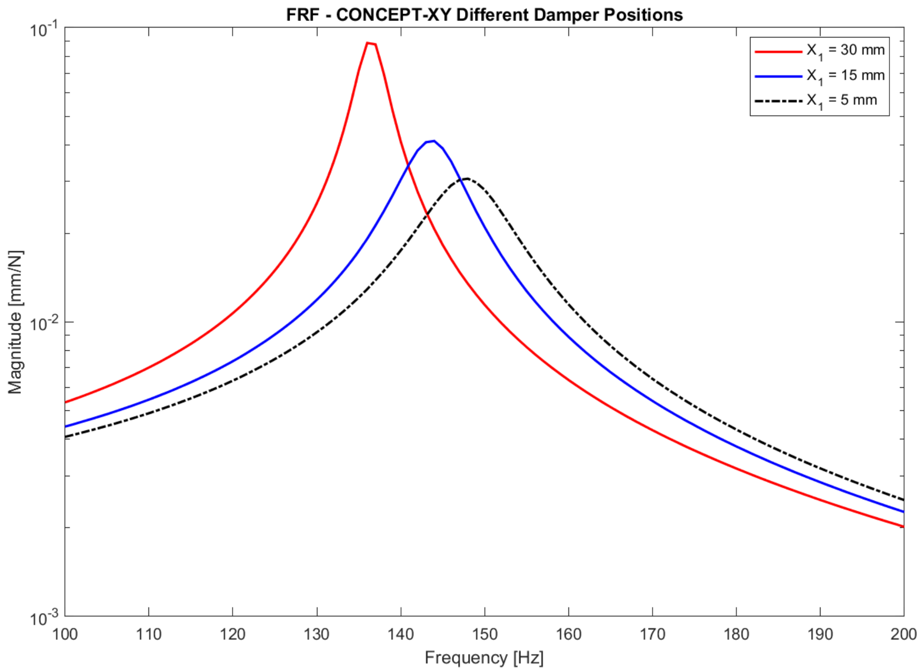

Figure 3.39: CONCEPT-XY with Different Damper Positions

3.3.1.6 Effect of Dividing The Damper Element

In order to determine whether a single long-link damper structure connected to the same regions or two short-link damper structures are more effective in providing damping, equal outer diameter and VEM thickness designs were created for both CONCEPT-XY and CONCEPT-YZ concepts, connected to the same regions. These designs are shown in Figures 3.40 - 3.43.

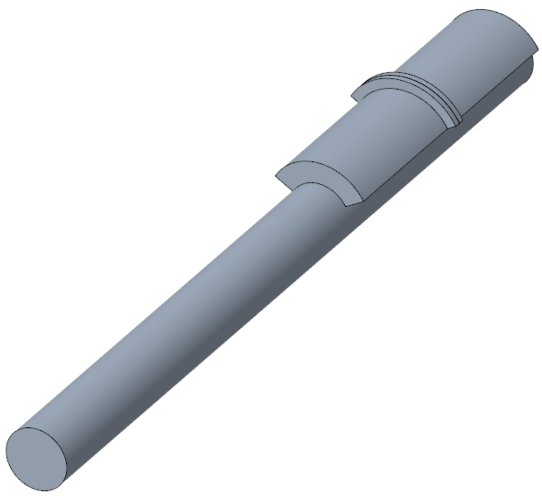

Figure 3.40: CONCEPT-XY with One Piece Damper

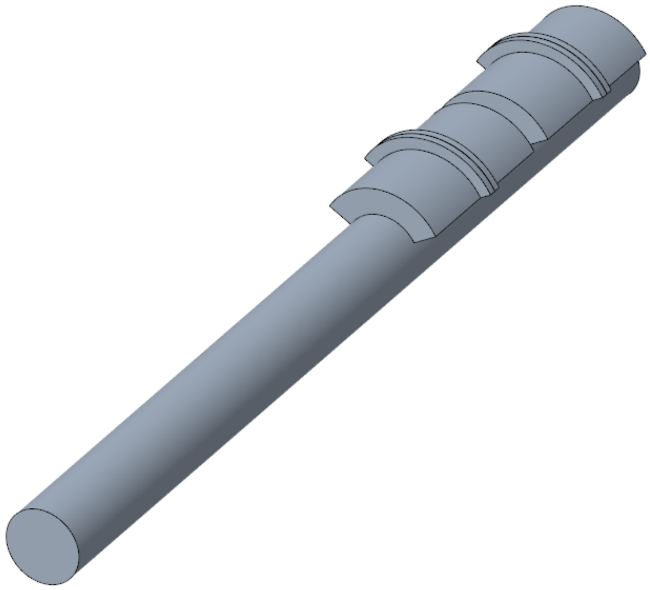

Figure 3.41: CONCEPT-XY with Two Pieces Damper

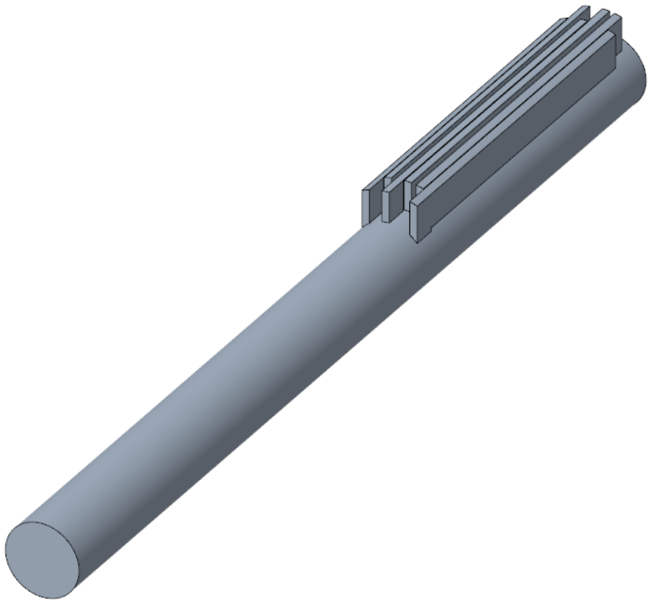

Figure 3.42: CONCEPT-XY with One Piece Damper

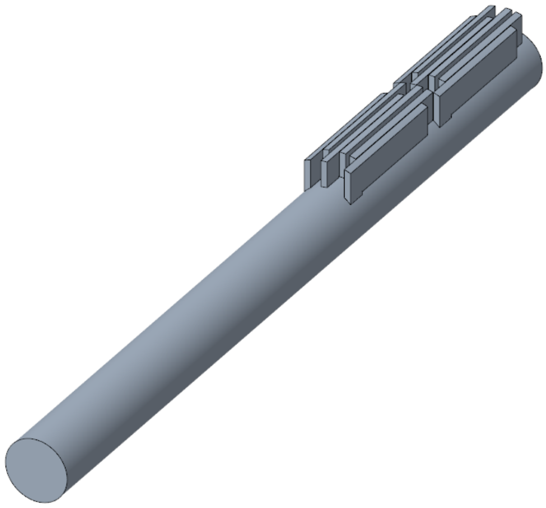

Figure 3.43: CONCEPT-XY with Two Pieces Damper

Harmonic Response Analysis was performed for these designs, and the free-end FRFs were calculated. The results are presented in Figure 3.44. As indicated by the results, using a single long link provides better performance and reduces vibration amplitude more effectively. Therefore, in the ongoing designs, dampers will be used as single units without division.

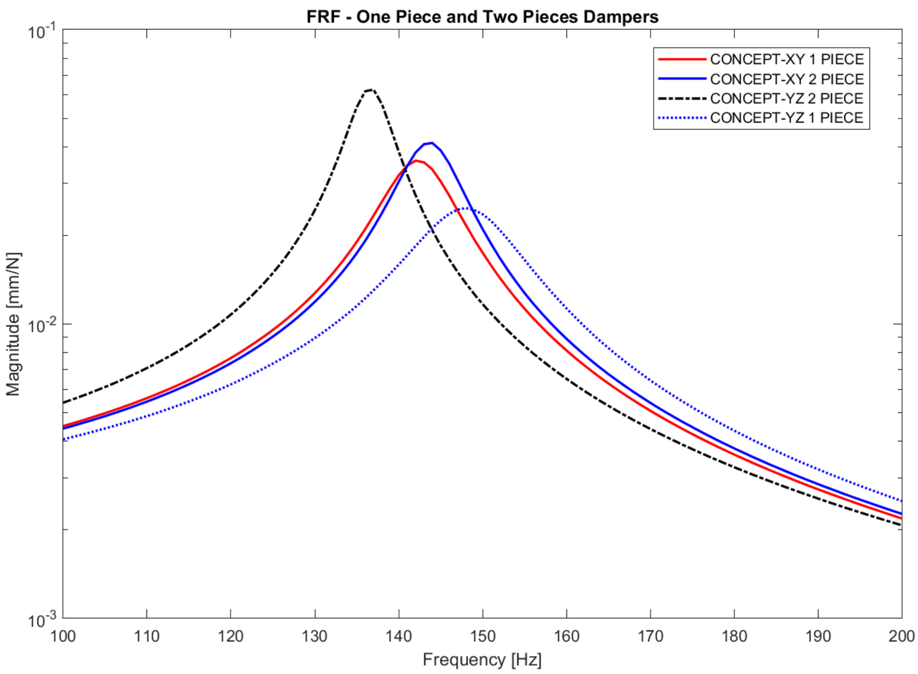

Figure 3.44: FRFs Comparison of One Piece and Two Pieces Dampers

3.3.1.7 Effect of Using Dampers of Both Side

Up to this point, the designs have placed viscoelastic dampers on a single surface. To investigate the impact of having dampers on both sides, CONCEPT-YZ dampers were symmetrically positioned on both sides of the boring bar. The resulting design is depicted in Figure 3.45, and its comparison with the design featuring dampers on a single side is provided in Figure 3.46. The results have clearly demonstrated that having dampers on both sides improves performance. In the final designs, the dampers will be positioned on both sides.

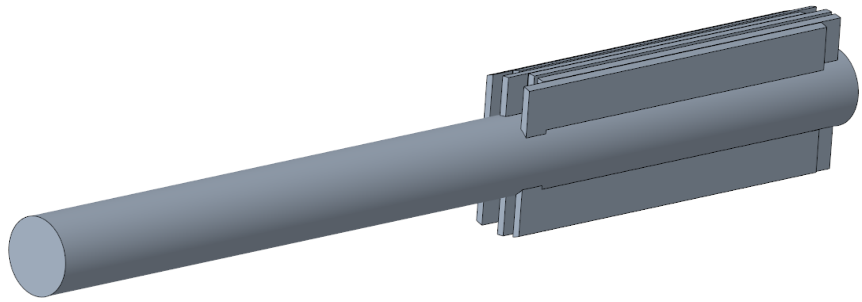

Figure 3.45: CONCEPT-YZ Double Sided

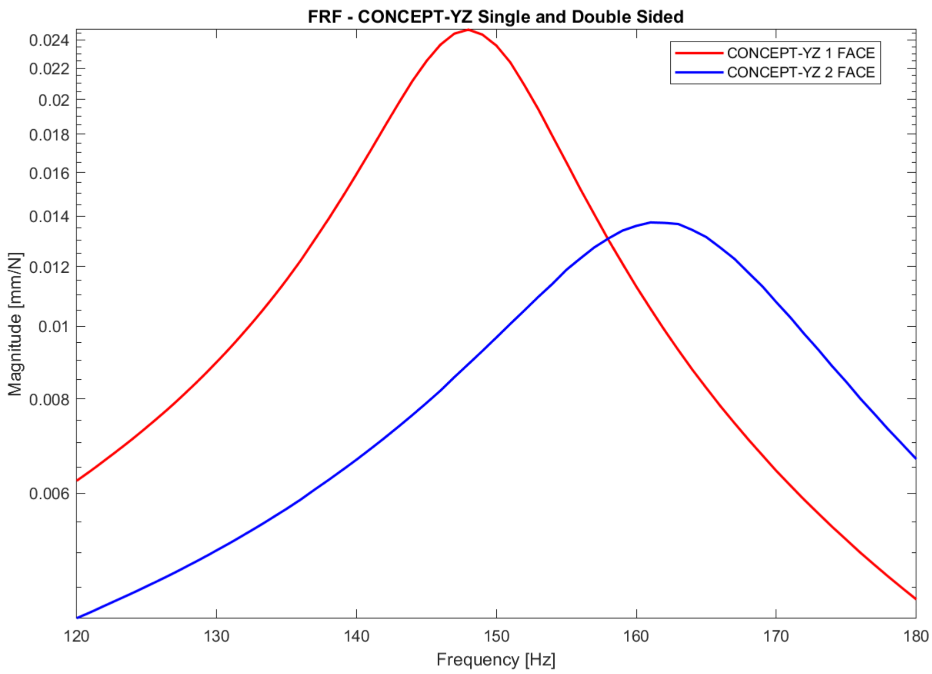

Figure 3.46: FRFs of CONCEPT-YZ Single and Double Sided

3.3.1.8 Selection of Best Concepts

Before starting the optimization studies, we had to narrow down the focus to the top two design concepts. To determine these concepts, we compared three different designs: CONCEPT-XY, CONCEPT-YZ, and CONCEPT-XZ dampers. All these dampers were placed at the same positions, had equal outer diameters, and viscoelastic material thickness. The comparison was based on the Frequency Response Function (FRF) results, which are presented in Figure 3.47.

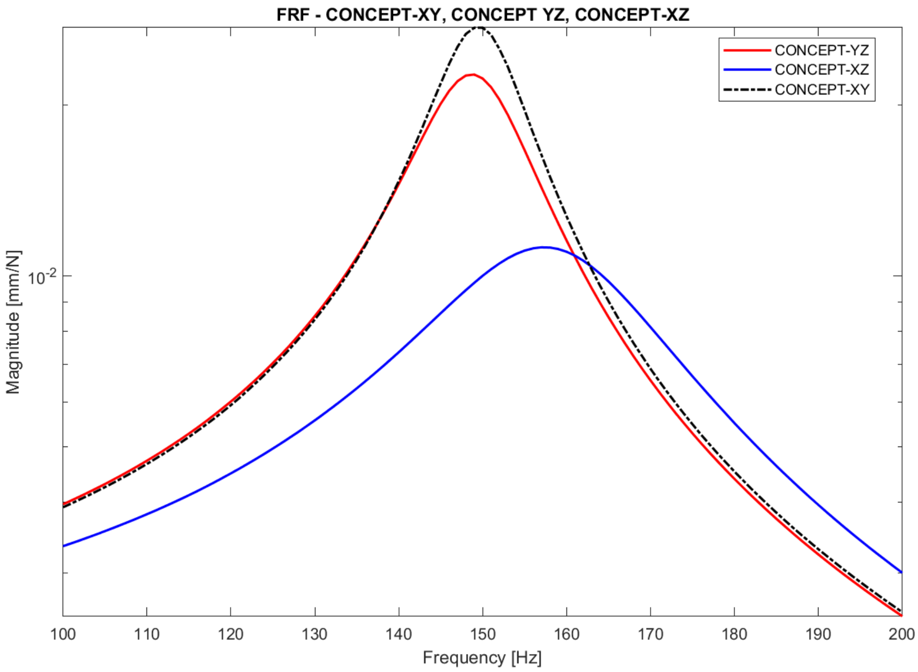

Figure 3.47: FRFs of CONCEPT-XY, CONCEPT-YZ and CONCEPT-XZ

As seen in the results in Figure 3.47, CONCEPT-YZ and CONCEPT-XZ dampers emerged as the top-performing options. They demonstrated better damping characteristics and reduced the vibration amplitudes significantly. Therefore, we decided to proceed with the optimization studies for these two concepts only. It is expected that the optimized design will have improved damping efficiency and reduced vibration levels, which will enhance the overall performance of the system.

3.3.2 Optimization of Conceptual Designs

To improve performance and achieve the best possible results, it is essential to use dampers in optimal geometries and positions. Based on the analyses conducted in the concept designs, optimization studies will be conducted with the two most promising concepts, and the optimized configurations of these two concepts will be compared. Figure 3.47 showed that CONCEPT-XZ and CONCEPT-YZ are the most promising concepts, and the comparison of these concepts against with bare beam is shown in Figure 3.48.

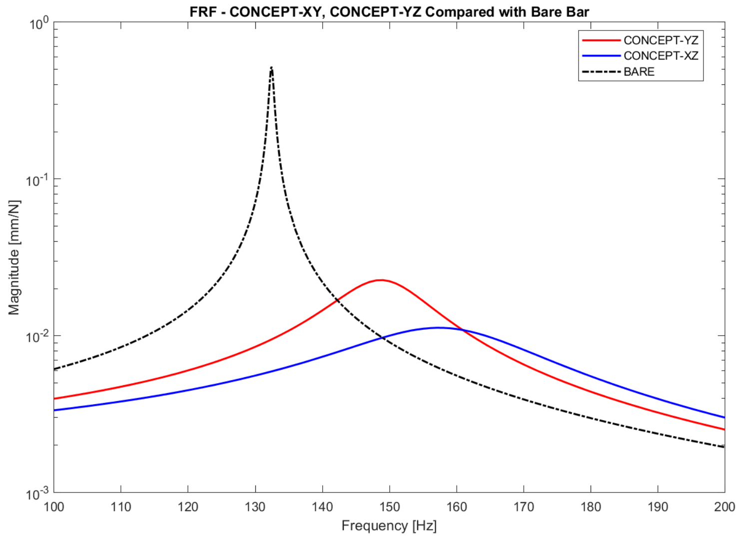

Figure 3.48: FRFs of CONCEPT-XY, CONCEPT-YZ Compared with Bare Bar

As seen from Figure 3.48, CONCEPT-XZ provides 90% lower peak amplitude compared to the bare boring bar while CONCEPT-YZ provides 83%. To improve these concepts and obtain optimum damper configurations, optimization studies will be conducted. Previous analyses that are conducted in this thesis have demonstrated that damper performance is highly dependent on geometries. Therefore, optimization studies involving link length, maximum outer diameter, and VEM thickness will be conducted with the goal of achieving the most optimal design.

When conducting the analyses, steel was assigned as the material for both the boring bars and links. The material properties assigned are provided in Table 3.4. To ensure realistic analysis results and enable accurate comparisons, an appropriate damping needed to be added to the material of the undamped boring bar. The suitable constant loss factor was determined to be $\gamma \approx 0.015$ from the FRF graphs found by using the half power point method in the studies of Zyl [45] and Grossi [29]. Therefore, in the analyses, for the undamped boring bar, a constant loss factor of 0.015 was input using ANSYS APDL commands. The analyses were conducted based on this boring bar.

Table 3.4: Material Properties of Steel

Property	**Value**
Density	7850 kg/m^3
Young's Modulus	200 GPa
Poisson's Ratio	0.3

The viscoelastic material used in the analyses is 3M 467MP, with a specified layer thickness of 0.06mm. To enhance adhesion performance and strength, at least two layers of VEM will be used. Therefore, the minimum VEM thickness is determined to be 0.12mm. In the optimization studies, the VEM thickness will initially be kept constant at this minimum value. As previously decided, dampers for both concepts will be attached 5mm inside from the fixed end. Subsequently, various link lengths and outer diameters are analyzed to create design matrices, leading to the determination of the optimal configuration for both concepts. The design matrices are presented in Table 3.5 and Table 3.6. In these tables, the tip point FRF peak amplitudes are compared.

Table 3.5: Peak FRF Amplitudes [mm/N] for CONCEPT-YZ with Different Link Heights and Lengths

LINK LENGTH [mm]	**OUTER DIAMETER [mm]**					
	45	50	55	60	65	70
100	4.35E-02	3.48E-02	3.13E-02	3.04E-02	3.10E-02	3.18E-02
150	2.85E-02	2.31E-02	2.15E-02	2.18E-02	2.32E-02	2.45E-02
200	2.57E-02	2.13E-02	**2.03E-02**	2.09E-02	2.25E-02	2.42E-02
250	2.78E-02	2.35E-02	2.26E-02	2.35E-02	2.51E-02	2.69E-02
300	3.26E-02	2.85E-02	2.75E-02	2.84E-02	3.02E-02	3.20E-02

Table 3.6: Peak FRF Amplitudes [mm/N] for CONCEPT-XZ with Different Link Heights and Lengths

LINK LENGTH [mm]	OUTER DIAMETER [mm]					
	45	50	55	60	65	70
100	2.93E-02	2.56E-02	2.38E-02	2.04E-02	2.39E-02	2.57E-02
150	1.86E-02	1.66E-02	1.59E-02	1.61E-02	1.73E-02	1.93E-02
200	1.69E-02	1.53E-02	**1.49E-02**	1.53E-02	1.66E-02	1.85E-02
250	1.88E-02	1.72E-02	1.69E-02	1.73E-02	1.86E-02	2.04E-02
300	2.31E-02	2.15E-02	2.09E-02	2.10E-02	2.18E-02	6.12E-02

For both concepts, the best results were obtained with a 55 mm diameter and a 200 mm link length, with the CONCEPT-XZ concept yielding superior results. While utilizing links of these dimensions, CONCEPT-XZ provides a 91% lower FRF peak magnitude compared to the bare beam, whereas CONCEPT-YZ provides a 88% reduction. The concepts that yield the best results are illustrated in Figure 3.49 and Figure 3.50.

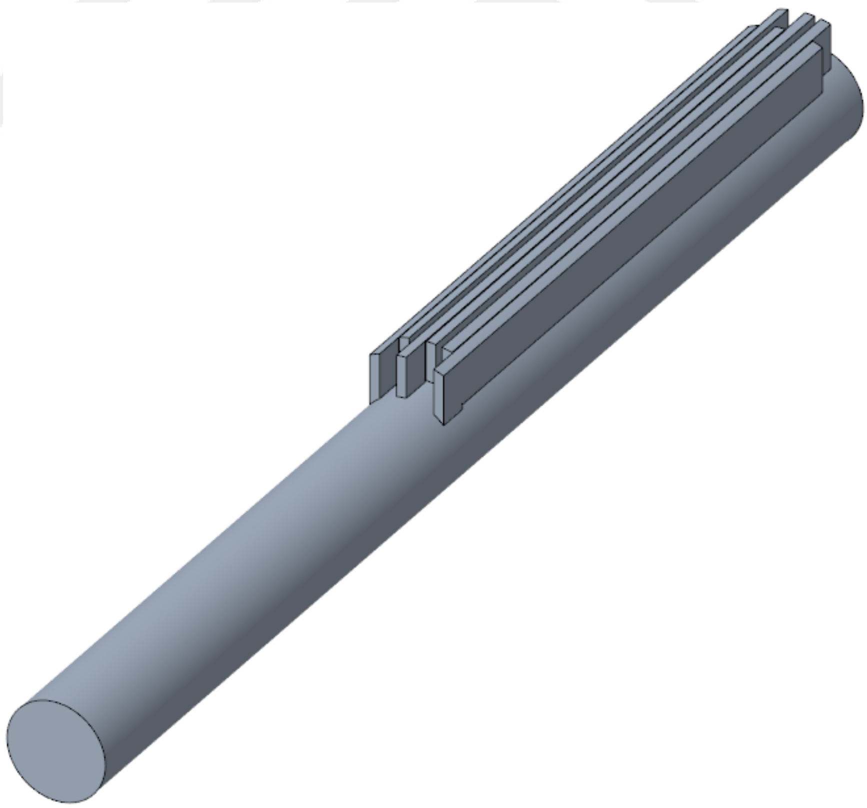

Figure 3.49: CONCEPT-YZ ⌀ = 55mm L = 200mm

Following this study, analyses were conducted for different VEM thicknesses to find

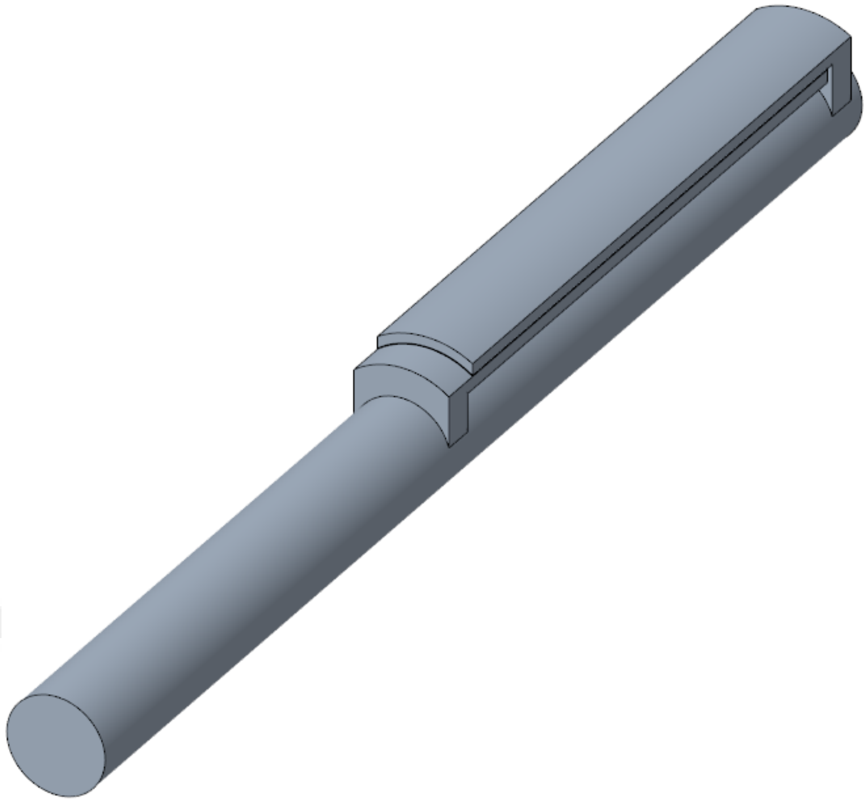

Figure 3.50: CONCEPT-XZ ⌀ = 55mm L = 200mm

the optimal VEM thickness for the 55mm diameter and 200mm link length, which produced the best results. During this optimization, VEM thickness steps were taken in increments of 0.06mm, which is the layer thickness of 3M 467MP. The results of the analyses for both concepts are provided in Tables 3.7 and 3.8.

Table 3.7: Peak FRF Amplitudes [mm/N] for CONCEPT-YZ with Different VEM Thickness

L=200 mm	**VEM THICKNESS [mm]**				
⌀=55 mm	0.12	0.18	0.24	0.3	0.36
AMP. [mm/N]	2.03E-02	1.84E-02	**1.79E-02**	1.81E-02	1.87E-02

Table 3.8: Peak FRF Amplitudes [mm/N] for CONCEPT-XZ with Different VEM Thickness

L=200 mm	**VEM THICKNESS [mm]**				
⌀=55 mm	0.12	0.18	0.24	0.3	0.36
AMP. [mm/N]	1.49E-02	1.37E-02	**1.35E-02**	1.38E-02	1.50E-02

The analyses resulted in the optimal VEM thickness for both concepts being 0.24mm. During the concept design stages, it was demonstrated that adding dampers to both sides of the boring bar yielded better results. Therefore, designs were created for both concepts with dampers added to both sides of the bar at the optimal dimensions (D=55mm L=200mm VEM T=0.24mm), as depicted in Figure 4.1 and Figure 4.2. The FRF graphs of the optimized concepts and the undamped bar are presented in Figure 3.53. The peak point FRF amplitudes and resonance frequencies are compared in Table 3.9.

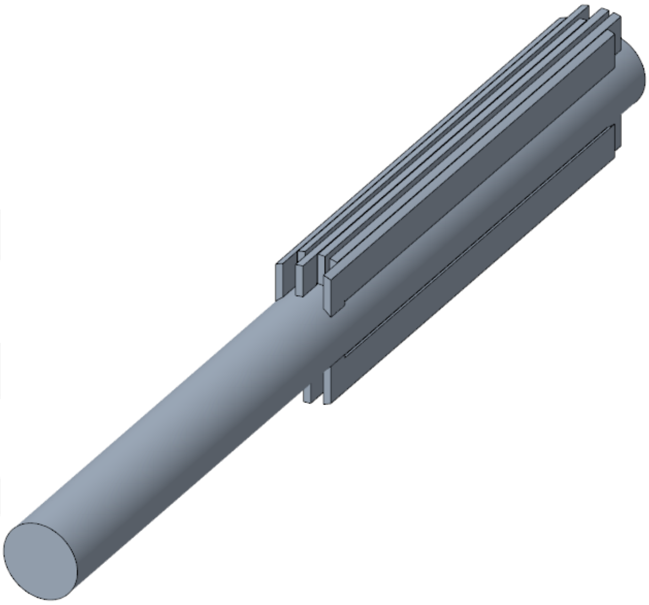

Figure 3.51: CONCEPT-YZ Double Sided ⌀ = 55mm L = 200mm VEMT = 0.24mm

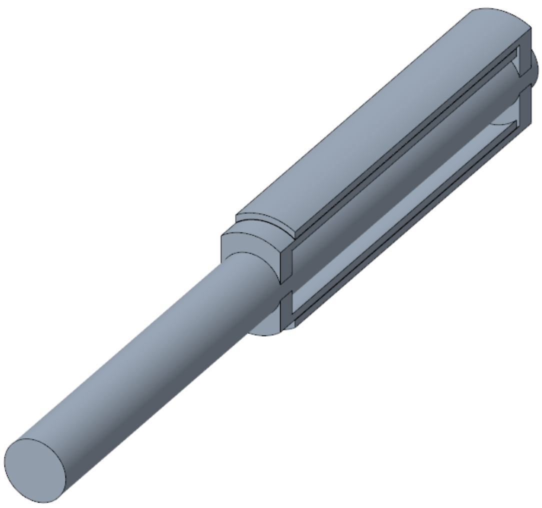

Figure 3.52: CONCEPT-XZ Double Sided ⌀ = 55mm L = 200mm VEMT = 0.24mm

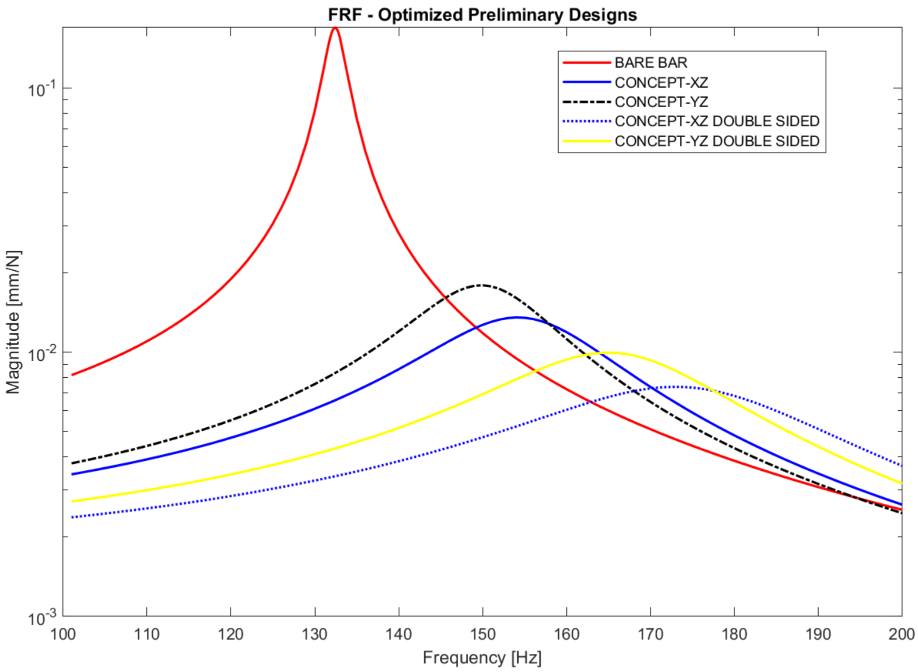

Figure 3.53: FRF Comparison of Optimized Preliminary Designs

Table 3.9: Optimized Dampers Performance

CONCEPT	PEAK AMP. (mm/N)	RES. FREQ [Hz]	RED. FOLD
BARE BAR	1.69E-01	134	NA
CONCEPT-YZ SINGLE SIDED	1.79E-02	150	9.44
CONCEPT-XZ SINGLE SIDED	1.35E-02	155	12.52
CONCEPT-YZ DOUBLE SIDED	9.94E-03	165	16.98
CONCEPT-XZ DOUBLE SIDED	**7.38E-03**	**173**	**22.88**

In this chapter, the concept of viscoelastic dampers was explained, and conceptual designs were developed for application to boring bars. From these conceptual designs, optimization studies were conducted for integration onto a 30 mm diameter and 400 mm length bare beam for CONCEPT-YZ and CONCEPT-XZ. From findings in optimization studies, 0.24 mm VEM thickness is optimum to damp boring bar vibrations (Table 3.7 and Table 3.8). Also, Table 3.9 shows that CONCEPT-XZ is the superior damper configuration up to now. If it is added to both two surfaces of the bar, provides a 22.88 times reduction compared with the bare boring bar. Also, double sided CONCEPT-YZ provides 16.98 times reduction in tip point FRF peak amplitude.

CHAPTER 4

OPTIMIZATION OF VISCOELASTIC DAMPER PARAMETERS FOR DIFFERENT SCENARIOS

In chapter 3, it is shown that proposed VEM damper designs provide an important amount of decrease in peak amplitudes of the tip FRFs. Thus an important amount of increase in productivity can be obtained by using the VEM dampers in boring bars. Viscoelastic dampers added to boring bars may increase the outer diameter of the tool. Following the optimization in conceptual designs, which has resulted in an increased maximum outer diameter of 55mm as shown in Figure 4.2 and Figure 4.1, it becomes apparent that the damped boring bar would not allow the machining of a hole with the same diameter and length as the original 30mm diameter, 400mm long boring bar. Considering the operational nature of boring bars, where the bar enters the hole, this situation is anticipated to elevate the minimum hole diameter that a boring bar can effectively process. To address this challenge and ensure continued functionality, the design of dampened boring bars will be explored within the framework of three distinct scenarios, each warranting its own optimization strategy. This approach is crucial to adapt the design to the new specifications imposed by the optimization process and maximize the performance of the dampened boring bars in their respective configurations. This chapter will present and discuss the details of these investigations and the optimization of damped designs for various scenarios.

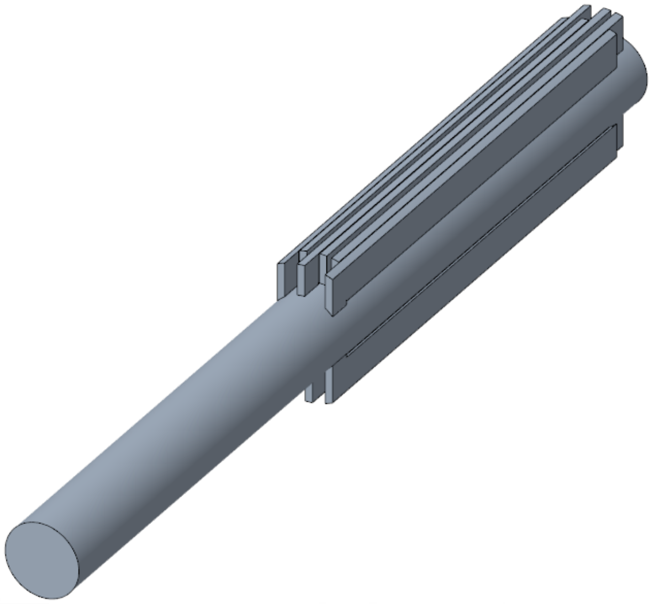

Figure 4.1: CONCEPT-YZ Double Sided ⌀ = 55mm L = 200mm VEMT = 0.24mm

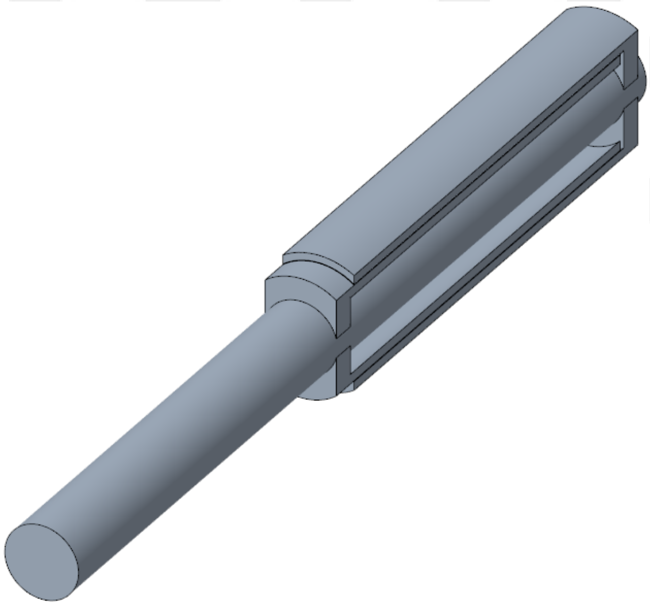

Figure 4.2: CONCEPT-XZ Double Sided ⌀ = 55mm L = 200mm VEMT = 0.24mm

4.1 Design Scenarios

The scenarios for utilizing viscoelastic dampers in boring bars have been elucidated in this section.

4.1.1 Scenario 1 - Maximum Damper Diameter Minimum Hole Diameter

In the first scenario, a design approach is considered where the maximum outer diameter of the dampened boring bar's viscoelastic dampers is kept smaller than the height of the inserts within the boring bar. A generic representation of this scenario is depicted in Figure 4.3. This configuration ensures that the dampened boring bar can fully enter the hole it is meant to machine, just like an undampened bare boring bar, and perform the necessary machining operations along its entire overhang length.

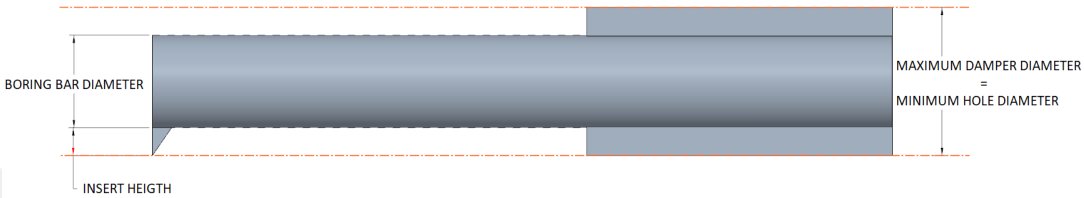

Figure 4.3: Damper Design Scenario - 1 and Design Parameters

4.1.2 Scenario 2 - Stepped Boring Bar

In the context of the study, the second scenario for dampened boring bar design introduces the concept of incorporating a step on the boring bar. This step provides a dedicated space for attaching the dampers. One of the key advantages of this approach is that it allows for a reduction in the diameter to which the dampers are connected, enhancing flexibility in their attachment points. This increased flexibility results in greater relative motion between the links, ultimately leading to improved damping performance.

To ensure that the dampers can be attached within the step while maintaining the required clearance from the machining surface, the maximum outer diameter of the dampers remains a critical consideration. This scenario's generic depiction can be observed in Figure 4.4.

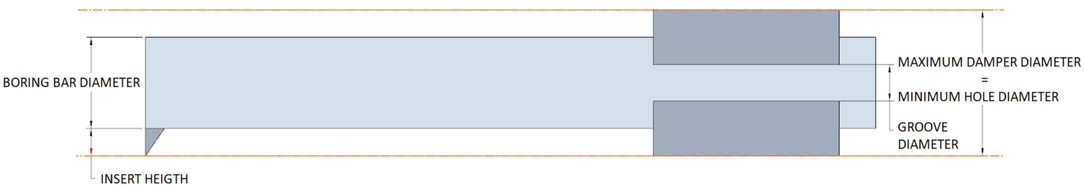

Figure 4.4: Damper Design Scenario - 2 and Design Parameters

4.1.3 Scenario 3 - Extra Damper Unit

In this scenario, the concept involves extending the effective length of the bare bar by adding an additional damping unit to it. The chosen length of the bare boring bar remains fixed, which is referred to as the "effective length." The idea is that this section can fit entirely within the hole being machined, and the portion with the dampers functions as an additional damping unit integrated into the boring bar. The scenario is depicted generically in Figure 4.5.

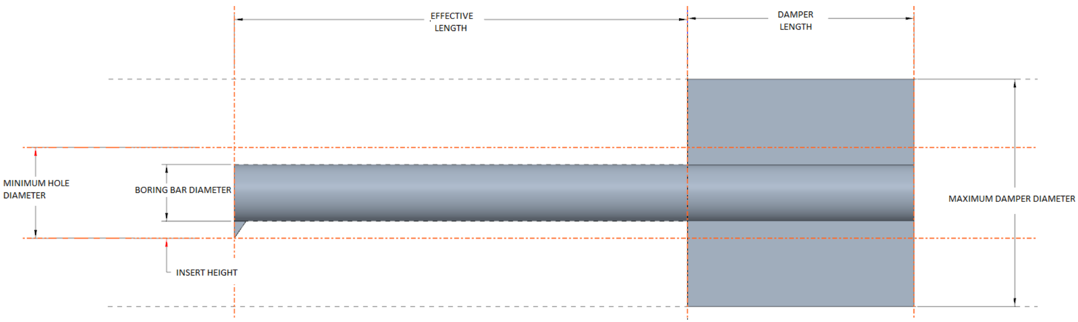

Figure 4.5: Damper Design Scenario - 3 and Design Parameters

4.2 Optimization of Viscoelastic Dampers for Different Designs Scenarios

The use of viscoelastic dampers in boring bars is described through three design scenarios. This section elucidates the optimization steps for each design scenario, and the optimizations of viscoelastic damper parameters are presented.

4.2.1 Optimization for Scenario - 1

This scenario was created by using the damper height not to be greater than the insert height. In order to develop suitable designs for this scenario, the optimized parameters of conceptual designs are taken as the starting point of the optimization. Given that the damping components' outer diameter has reached 55mm following the optimization, which required comparison to a boring bar with a minimum hole machining diameter of 55mm. When inspecting products from the well-known company SANDVIK, which manufactures widely-used boring bars, it was observed that boring bars with a 55mm minimum hole machining diameter (e.g., 825D-70TC11U-C5M and

825D-70TC11U-C6M) have a boring bar body diameter of 50mm. Taking this information into account, the optimized designs were compared to a boring bar with a 50mm diameter and 400mm long. Additionally, 55mm outer diameter dampers with a link length of 200mm were applied to 40mm and 50mm diameter bare bars for further analysis. The performance comparison of these designs is presented in Table 4.1.

Table 4.1: Scenario - 1 Performance Comparison

CONCEPT	PEAK AMP. (mm/N)	RES. FREQ [Hz]	RED. FOLD
BARE BAR 50MM DIA	2.19E-02	222	NA
CONCEPT-YZ 30MM BARE DIA	1.79E-02	150	1.22
CONCEPT-XZ 30MM BARE DIA	1.35E-02	155	1.62
CONCEPT-YZ DOUBLE SIDED 30MM BARE DIA	9.94E-03	165	2.20
CONCEPT-XZ DOUBLE SIDED 30MM BARE DIA	7.38E-03	173	2.97
CONCEPT-YZ DOUBLE SIDED 50MM BARE DIA	5.35E-03	210	4.09
CONCEPT-XZ DOUBLE SIDED 50MM BARE DIA	5.45E-03	236	4.02
CONCEPT-YZ DOUBLE SIDED 40MM BARE DIA	4.90E-03	199	4.47
CONCEPT-XZ DOUBLE SIDED 40MM BARE DIA	**3.89E-03**	**206**	**5.63**

As seen from Table 4.1, a dampened boring bar with CONCEPT-XZ dampers applied to both sides of a 40 mm diameter bare bar can reduce the resonance peak amplitude by a factor of 5.63 when compared to a 50 mm diameter, 400 mm long bare boring bar. It is shown in Figure 4.6. Also, the tip point FRF results of the optimum design for that scenario and 50 mm diameter bare boring bar are shown in Figure 4.7

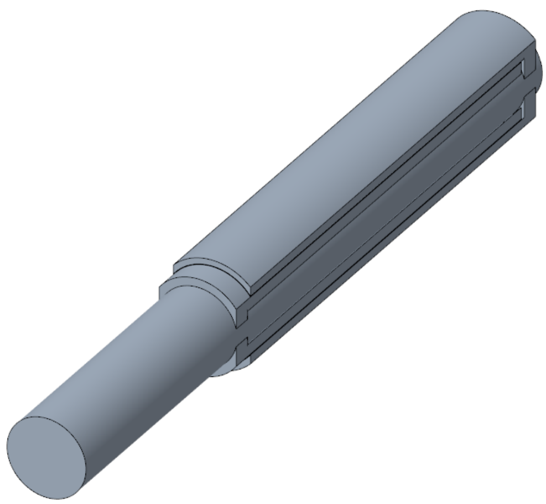

Figure 4.6: Solid Model of CONCEPT-YZ Double Sided Applied to 40 mm Bare Diameter (Best Design of Scenario - 1)

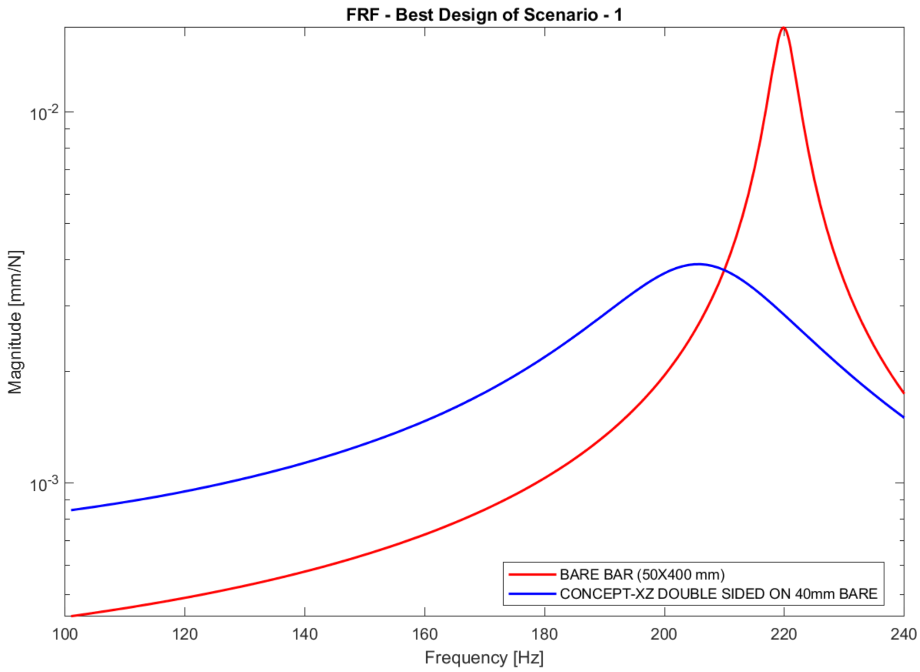

Figure 4.7: FRF of Best Design of Scenario - 1 (CONCEPT-YZ Double Sided Applied to 40 mm Bare Diameter)

4.2.2 Optimization for Scenario - 2

In the second scenario, a slot will be opened in the area where the dampers will be applied to reduce the diameter of the boring bar, and dampers will be added. For this scenario, the outer diameter is held constant, while the step diameter and link lengths serve as variable parameters in the optimization process. The optimization work has been conducted for both the CONCEPT-XZ and CONCEPT-YZ designs. In the analysis model, dampers were integrated onto a stepped 50mm diameter, 400 mm long bare boring bar, with the dampers featuring a fixed outer diameter of 55mm.

The optimization process for both design concepts, CONCEPT-XZ and CONCEPT-YZ, was carried out using ANSYS Harmonic Response Analysis. The key results of this optimization have been documented and are presented in Tables 4.2 and 4.3. These tables showcase the peak values at the endpoint of the optimal dampers' frequency response functions.

Subsequently, these values were compared to those obtained from a 50 mm diameter, 400 mm long bare boring bar. Tip point FRF graphs are represented in Figure 4.8 and

Table 4.2: Peak FRF Amplitudes [mm/N] for CONCEPT-YZ with Different Step Diameter and Link Lengths

LINK LENGTH [mm]	STEP DIAMETER [mm]		
	35	40	45
200	6.33E-03	6.15E-03	6.95E-03
225	6.26E-03	**6.02E-03**	6.77E-03
250	6.45E-03	6.12E-03	6.79E-03

Table 4.3: Peak FRF Amplitudes [mm/N] for CONCEPT-XZ with Different Step Diameter and Link Lengths

LINK LENGTH [mm]	STEP DIAMETER [mm]		
	35	40	45
200	5.55E-03	4.33E-03	3.66E-03
225	5.49E-03	4.32E-03	**3.58E-03**
250	5.95E-03	4.49E-03	3.68E-03

the comparative peak point amplitude results are detailed in Table 4.4.

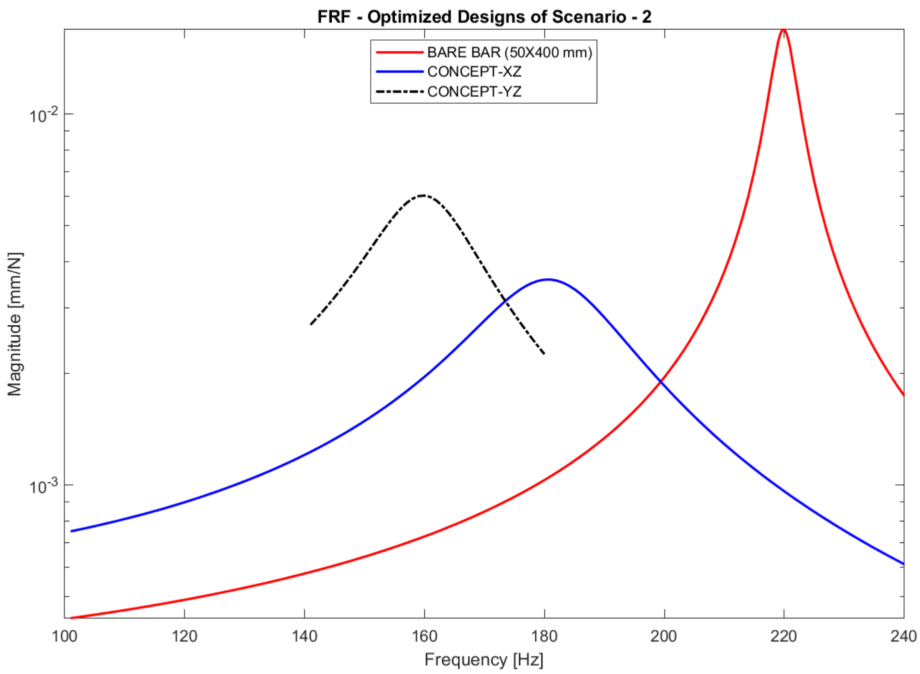

Figure 4.8: FRF of Optimized Designs for Scenario - 2

Table 4.4: Scenario - 2 Performance Comparison

CONCEPT	PEAK AMP. (mm/N)	RES. FREQ. [Hz]	RED. FOLD
BARE BAR 50MM DIA	2.19E-02	222	NA
CONCEPT-YZ DOUBLE SIDED 40MM STEP	6.02E-03	160	3.64
CONCEPT-XZ DOUBLE SIDED 40MM STEP	**3.58E-03**	**181**	**6.12**

As seen from results given in Table 4.4, it is evident that the dampened boring bar, which integrates 40mm diameter step and 225mm link lengths for the CONCEPT-XZ dampers, is capable of reducing vibration amplitude by an impressive factor of 6.12 when compared to the bare boring bar counterpart. This conclusion also signifies that, considering both scenarios, the most effective design for a 400mm overhang length with a minimum hole diameter of 55mm is the one labeled as "CONCEPT-XZ DOUBLE SIDED 40MM STEP" That design is visually represented in Figure 4.9.

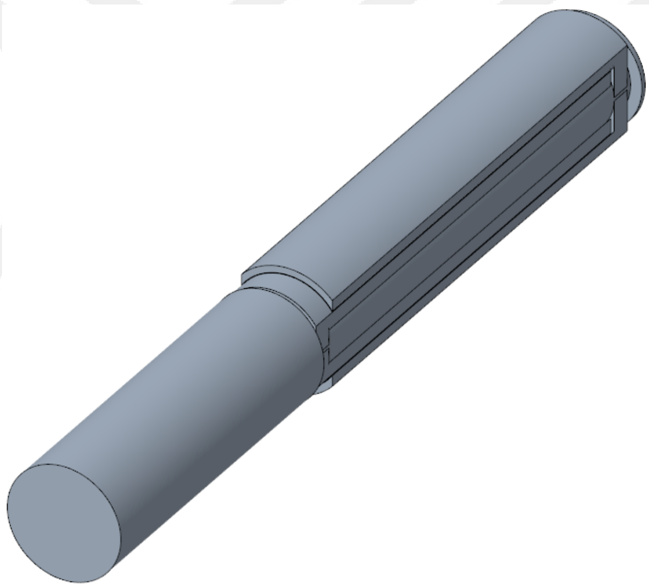

Figure 4.9: 50 mm Diameter Boring Bar with Double Sided CONCEPT-XZ Damper Added 40 mm Step

In this scenario, the concept created is applied to a bar with a diameter of 40mm and a length of 560mm for comparison with Zyl's study found in the literature [15]. The comparison results are given in the Chapter 6. In this application, considering the same insert height, the maximum outer diameter is kept at 45 mm. Optimization matrix is created for CONCEPT-XZ (Table 4.5 that gives better results. While the obtained FRF graph is shown in Figure 4.10, the comparison of the peak points of the

FRFs is provided in Table 4.6.

Table 4.5: Peak FRF Amplitudes [mm/N] for CONCEPT-XZ with Different Step Diameter and Link Lengths

LINK LENGTH [mm]	STEP DIAMETER [mm]		
	20	25	30
225	3.71E-02	2.53E-02	1.98E-02
250	3.59E-02	2.41E-02	1.86E-02
275	3.61E-02	2.38E-02	1.795E-02
300	3.74E-02	2.42E-02	**1.790E-02**

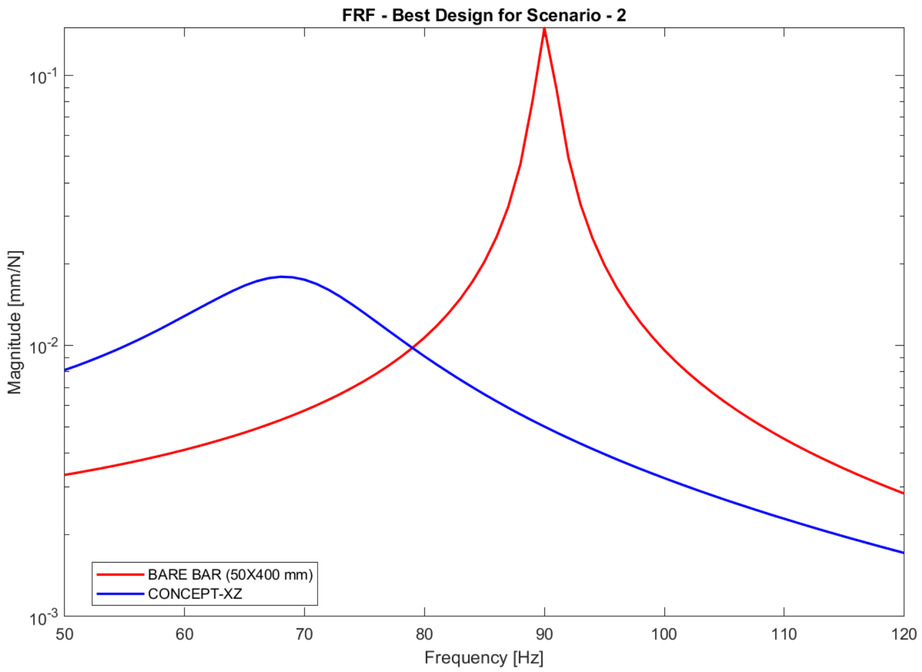

Figure 4.10: FRF of Best Design for Scenario - 2 (⌀40x560mm Bar)

Table 4.6: Scenario - 2 Performance Comparison (40X560)

CONCEPT	PEAK AMP. (mm/N)	RES. FREQ. [Hz]	RED. FOLD
BARE BAR 40MM DIA 560MM LENGTH	1.47E-01	91	NA
CONCEPT-XZ DOUBLE SIDED 40MM STEP	**1.79R-02**	**68**	**8.21**

As seen in Figure 4.10 and Table 4.6, it is evident that the dampened boring bar, which integrates 30 mm diameter step and 300 mm link lengths for the CONCEPT-XZ dampers, is capable of reducing vibration amplitude by an impressive factor of 8.21 when compared to the bare boring bar with 40 mm diameter and 560 mm length.

4.2.3 Optimization for Scenario - 3

In this scenario, a separate damper unit will be added as an extra unit instead of it entering the hole. For this scenario, a boring bar geometry with a 40mm diameter and a length of 560mm, resulting in an L/D ratio of 14, was selected. The aim is to reach an optimal solution by adding a damping unit to the chosen boring bar geometry while keeping the length of the bare portion constant. In both concepts, optimization was carried out for the outer diameter of the dampers and the link lengths. During the analyses, the VEM thickness was kept fixed at 0.24mm. The optimization results are presented in Table 4.7 and Table 4.8.

Table 4.7: CONCEPT-YZ Outer Diameter and Link Length Optimization

LINK LENGTH [mm]	**DIAMETER [mm]**		
	60	70	80
200	5.57E-02	4.45E-02	4.35E-02
250	5.29E-02	**4.31E-02**	4.34E-02
300	5.41E-02	4.42E-02	4.57E-02

Table 4.8: CONCEPT-XZ Outer Diameter and Link Length Optimization

LINK LENGTH [mm]	**DIAMETER [mm]**		
	60	70	80
200	4.26E-02	3.72E-02	3.80E-02
250	4.00E-02	**3.43E-02**	4.06E-02
300	4.10E-02	3.68E-02	3.96E-02

As the results given in Table 4.7 and Table 4.8 demonstrate, the design that achieved the best performance for this scenario dampers with a 70 mm outer diameter, and a 250 mm link length, applied to both sides of the boring bar for both CONCEPT-XZ and CONCEPT-YZ. The tip point FRF graphs of these design are presented in Figure 4.11 with bare boring bar FRF.

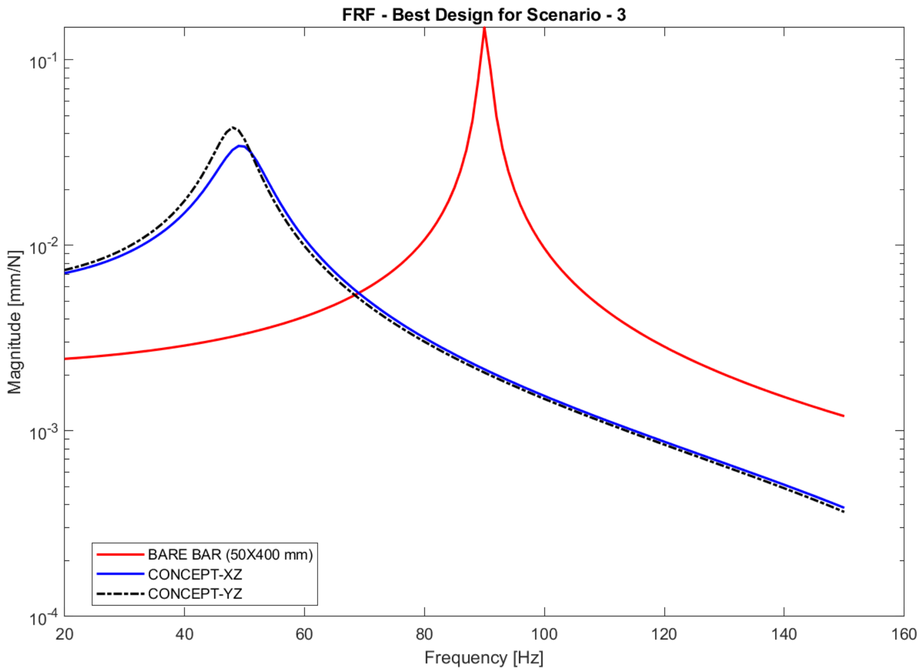

Figure 4.11: FRF of Best Design for Scenario - 3 (⌀40x560 mm Bar)

Figure 4.11 shows that the boring bar with CONCEPT-XZ dampers provides more damping compared to CONCEPT-YZ. The design that yielded the best results is shown in Figure 4.12.

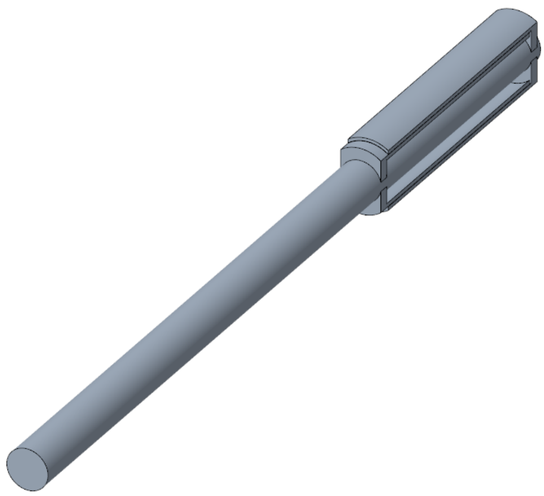

Figure 4.12: Double Sided CONCEPT-XZ Damper Added to ⌀40x560 mm Bare Bare

In this scenario, another design is created using CONCEPT-XZ dampers. In the created design, the connection diameter of the boring bar has been increased, and the rigid link closer to the fixed end is connected to this larger diameter. For this design, three different design matrices were created with connection diameters of 60 mm, 70 mm, and 80 mm, and optimization studies were conducted as shown in Table 4.9, 4.10 and 4.11.

Table 4.9: Peak FRF Amplitudes [mm/N] for CONCEPT-XZ with Different Outer Diameter and Link Length (Connection Diameter=60 mm)

LINK LENGTH [mm]	**DIAMETER [mm]**		
	70	80	90
200	2.88E-02	2.73E-02	5.77E-02
250	2.73E-02	**2.66E-02**	4.06E-02
300	2.81E-02	2.77E-02	3.09E-02

Table 4.10: Peak FRF Amplitudes [mm/N] for CONCEPT-XZ with Different Outer Diameter and Link Length (Connection Diameter=70 mm)

LINK LENGTH [mm]	**DIAMETER [mm]**		
	70	80	90
200	2.60E-02	2.69E-02	3.09E-02
250	**2.52E-02**	2.69E-02	3.16E-02
300	2.62E-02	2.84E-02	3.49E-02

Table 4.11: Peak FRF Amplitudes [mm/N] for CONCEPT-XZ with Different Outer Diameter and Link Length (Connection Diameter=80 mm)

LINK LENGTH [mm]	**DIAMETER [mm]**		
	70	80	90
200	2.63E-02	2.91E-02	3.49E-02
250	**2.58E-02**	2.96E-02	3.65E-02
300	2.71E-02	3.16E-02	3.89E-02

The optimum design is the design that has dampers with 250 mm length and 80 mm outer diameter while connection diameter is 70 mm. As a result of reducing the amplitude by 5.83 times, this design has proven to be the optimal one for this scenario. It is illustrated in Figure 6.4. Comparative results for the obtained optimal design are shared in Table 4.12.

Table 4.12: Scenario - 3 Performance Comparison

CONCEPT	PEAK AMP. (mm/N)	RES. FREQ. [Hz]	RED. FOLD
BARE BAR 40MM x 560 MM	1.47E-01	91	NA
CONCEPT-YZ DOUBLE SIDED	4.31E-02	49	3.41
CONCEPT-XZ DOUBLE SIDED	3.43E-02	50	4.29
CONCEPT-XZ DOUBLE SIDED CON. DIA.= 70MM	**2.52E-02**	**53**	**5.83**

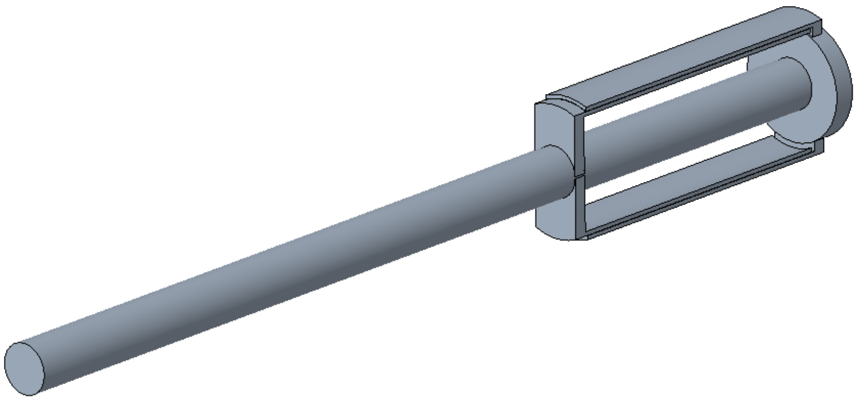

Figure 4.13: Solid Model of CONCEPT-XZ Double Sided Connection Diameter = 70 mm (Best Design for Scenario - 3)

As seen in Table 4.12, tip point FRF peak amplitude can be reduced 5.83 times compared to the bare boring bar in this scenario.

CHAPTER 5

EXPERIMENTAL VALIDATION

In Chapter 4, three different scenarios related to the use of viscoelastic dampers on boring bars were created, and the parameters of viscoelastic dampers were optimized for these scenarios. Through the optimization process using ANSYS Mechanical FEM analysis, the highest damping was achieved in Scenario-2. For Scenario-2, where designed a boring bar with steps and dampers were applied, the best result was obtained with CONCEPT-XZ (Figure 5.1).

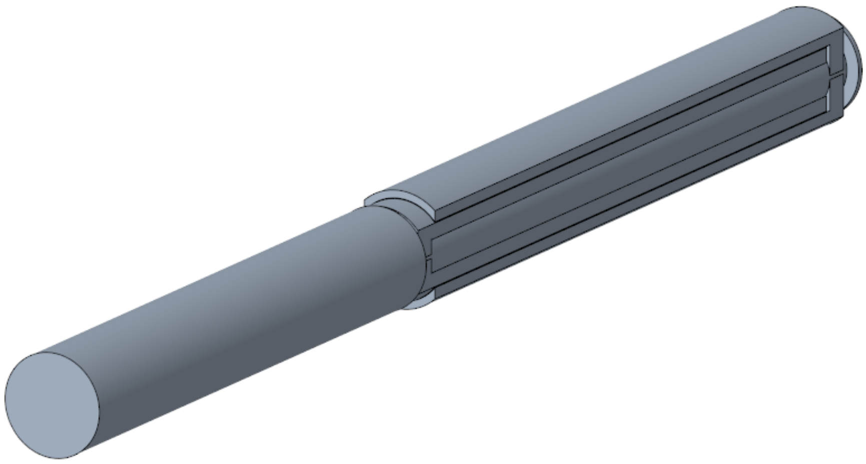

Figure 5.1: Solid Model of Best Design for Scenario - 2 (CONCEPT-XZ Added to 30 mm Step

5.1 Manufacturing of Optimum Design

This optimized design, analyzed and optimized through FEM analyses, will be experimentally validated. For the experiment, a bare bar with a diameter of 40 mm and a length of 660 mm was manufactured. Additionally, a base bar with a

30 mm diameter step, intended for damper attachment, was produced with the same dimensions. Due to the difficulty and lengthy production time of the circular structure links used in the analyses, flat links of the same dimensions were manufactured for model validation. A design has been created to allow rigid links to be bolted to the boring bar for a modular design. The design includes a bolted assembly of the dampened bar with flat links, as shown in Figure 5.2.

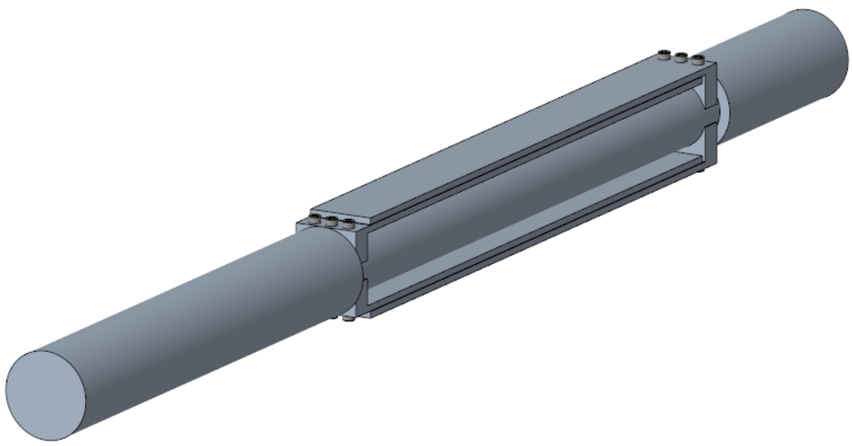

Figure 5.2: Solid Model of Damped Beam with Flat Links

To simplify the machining process, links were manufactured in two parts. Foot and flat layer of the link are separated from each other and manufactured separately. Manufactured flat links are represented in Figure 5.3. The base bar which has a step for dampers is shown in Figure 5.4 and the base bar with link feet is represented in Figure 5.5.

Figure 5.3: Manufactured Flat Links

Figure 5.4: Manufactured Base Bar

Figure 5.5: Manufactured Link Foot

After machining, to create damper units, 3M 468MP (Shown in Figure 5.6) is used which has same properties with 3M 467MP but only difference is the layer thickness of VEM. For 0.24mm thickness 2 layers 3M 468MP is used.

Figure 5.6: A Roll of 3M 468MP

Firstly, the viscoelastic material is applied to the flat links and waited for full adhesion and strength (Figure 5.7 and Figure 5.8). Then, the dampers bolted to the base bar with feet, as shown in Figure 5.9.

Figure 5.7: Flat Links with VEM

Figure 5.8: Flat Links with VEM

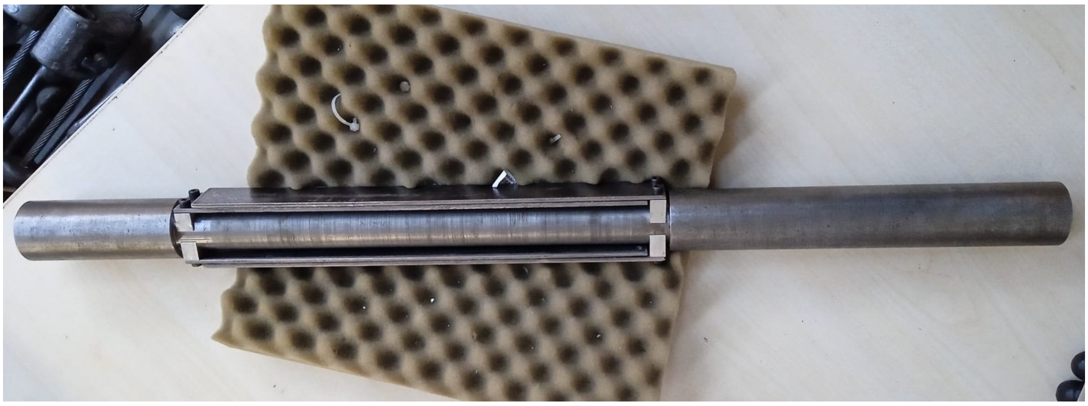

Figure 5.9: Damped Bar

5.2 Experiments

Damped and undamped bars which are produced are shown in Figure 5.10.

Figure 5.10: Manufactured Undamped and Damped Bars - 2

Initially, the undamped bar was mounted on the lathe with a 560 mm overhang length, as shown in Figure 5.11. A modal test was conducted using an accelerometer placed at the tip and a hammer. The obtained FRF graph is presented in Figure 5.12.

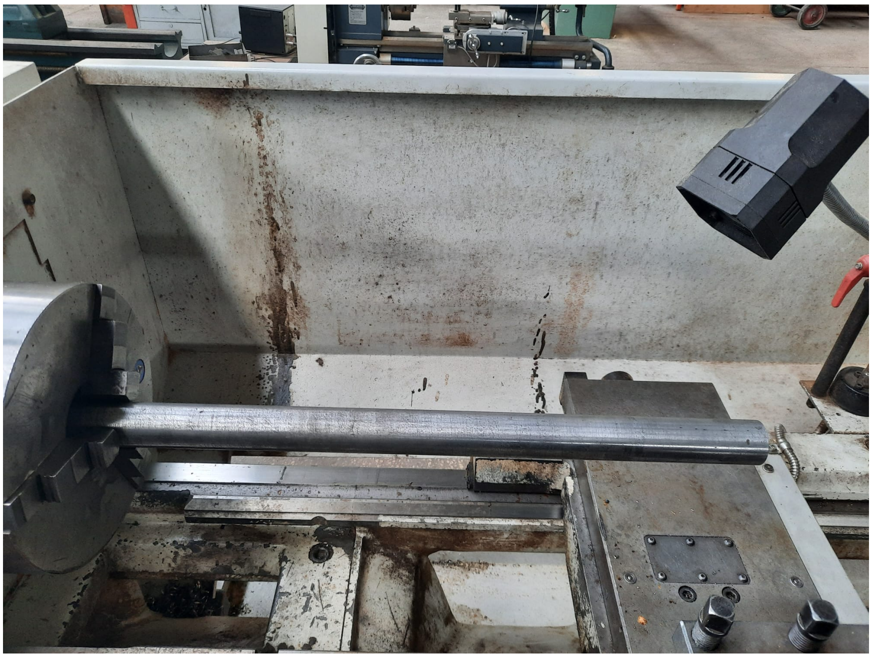

Figure 5.11: Bare Boring Bar Fixed to Lathe

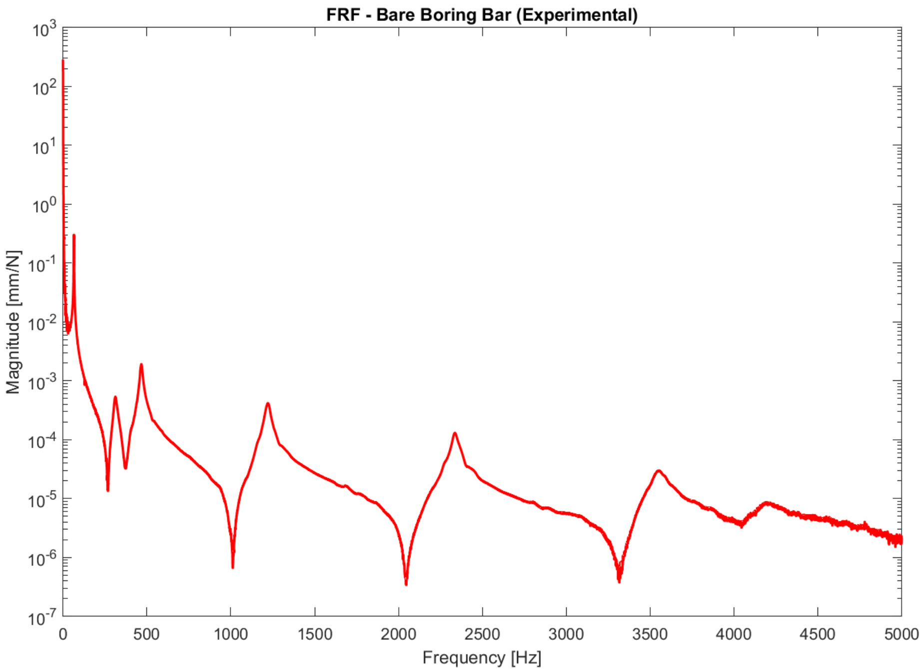

Figure 5.12: Bare Boring Bar Experimentally Obtained FRF

Due to the flexible connection in fixing the part to the lathe, the expected natural frequency of the first mode at approximately 90 Hz was observed as 65 Hz. Therefore, the part was reanalyzed in Ansys Mechanical by changing the boundary condition from Fixed to Elastic. Iterations were performed in modal analysis to determine the stiffness, aiming to achieve the experimentally obtained 65 Hz. The model and the appropriate stiffness value obtained experimentally are illustrated in Figure 5.13.

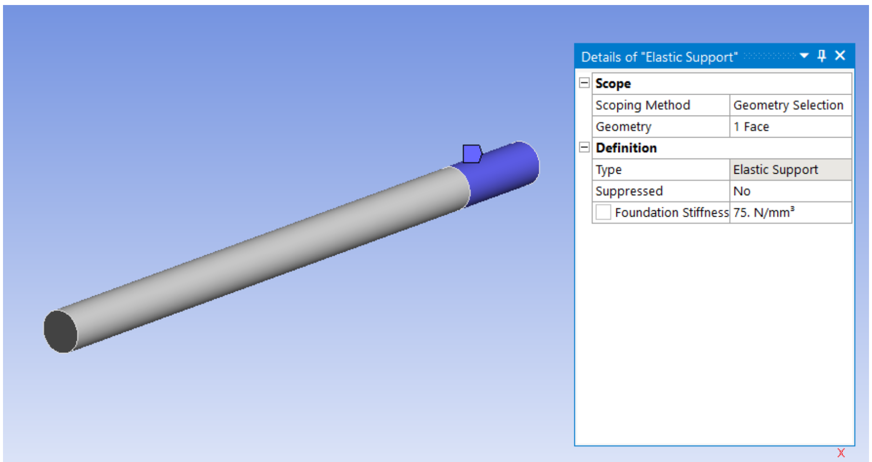

Figure 5.13: Bare Boring Bar Simulation Model with Elastic Boundary Condition

By using that boundary condition, harmonic analyses are run to decide the proper constant loss factor of the bare boring bar. Figure 5.14 shows FRF graphs of experimental and simulated bars with different constant constant loss factors near the resonance.

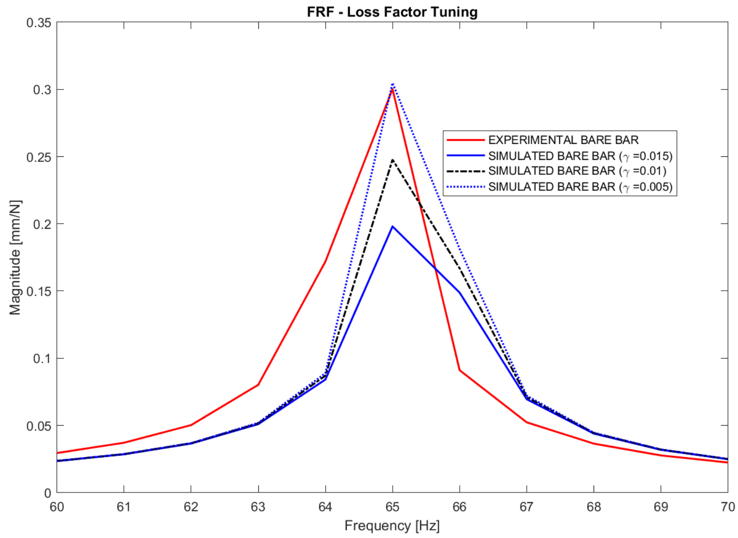

Figure 5.14: Bare Boring Bar FRFs with Different Loss Factor Values

As seen from Figure 5.14, constant loss factor 0.005 is proper to use, and the manufactured damped bar was analyzed with that elastic boundary condition and loss factor. The manufactured damped bar was also mounted on the lathe with a 560 mm overhang length (Figure 5.15). As seen in Figure 5.15, an accelerometer is placed near the tip point of the bar. Figure 5.16 shows the impact hammer, and Figure 5.17 shows the data acquisition product that was used in the experiments.

Figure 5.16: Impact Hammer

Figure 5.15: Damped Boring Bar Test Setup

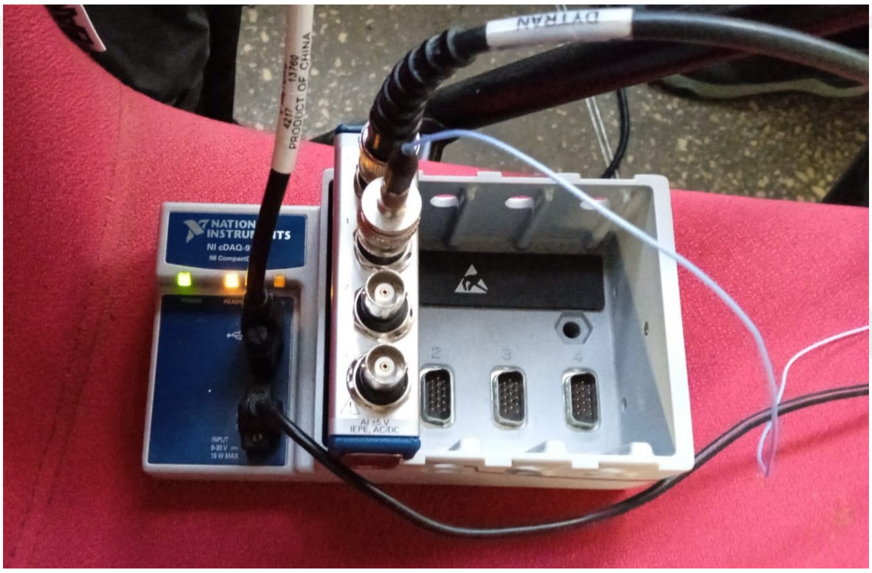

Figure 5.17: Data Acquisition System

5.3 Experimental Results

Figure 5.18 shows the FRF graphs of bare and damped beams obtained from both experiments and simulations.

As observed from Figure 5.18, there is a discrepancy between the experimentally obtained FRF for the damped bar and the simulated FRF. The peak point magnitude of the FRF, which appears to be reduced by 7 times according to the simulation data, is actually reduced by 3.66 times in experimental studies. This difference

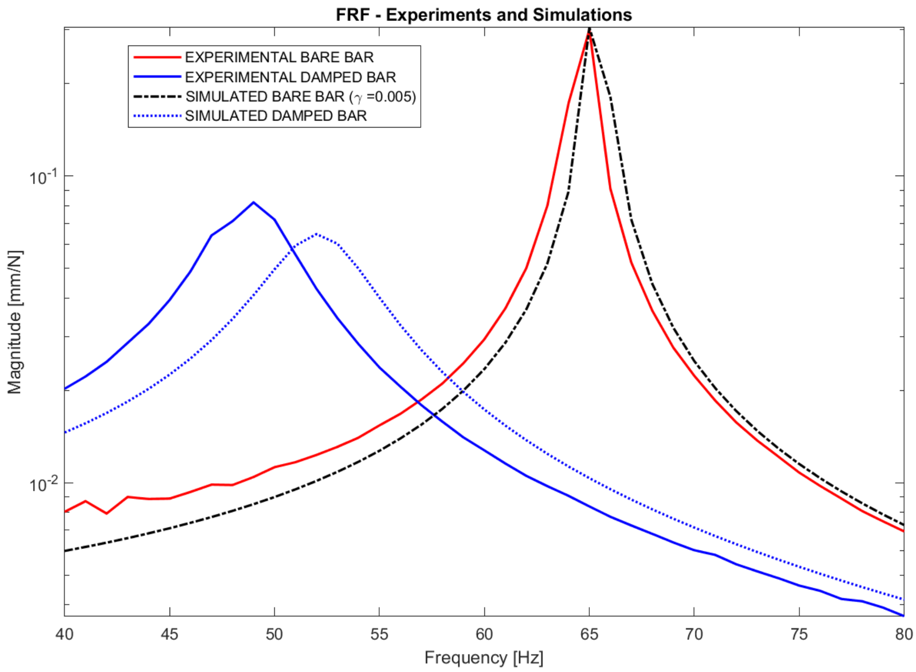

Figure 5.18: FRF Results of Experiments and Simulations

may arise from the fact that the bolted assembly condition, with separate link feet inserted, may not entirely create a bonded boundary condition. Also, the boundary condition of fixed side is not exactly modelled. In experiment, the chuck has three point contacts and it is not symmetric exactly. In simulation model, elastic boundary condition applied to a whole cylindrical surface. In addition to these reasons, simulations are made for 25 degrees Celsius environment temperature. However, there is approximately 15 degrees Celsius environment temperature where experiment is done. Due to the temperature sensitive nature of viscoelastic materials, it could affect the damping performance and stiffness of damping material. Also, due to manufacturing errors, flat plates could not be manufactured as flat as required. It causes some adhesion problems at the ends of the flat plates, and effective viscoelastic material length is decreased. It affects the damping performance negatively.

CHAPTER 6

RESULTS AND ANALYSIS

6.1 Stability Lobe Diagrams

After analyzing the data, the design with the highest reduction in FRF peak amplitude was obtained by using CONCEPT-XZ dampers, as described in Scenario 2. This concept achieved an 8.21 times reduction in FRF peak amplitude compared to the boring bar without dampers. The FRF amplitude was used in the design and optimization studies. However, according to the linear stability theory, it is known that the limit depth of cut is inversely proportional to the real part of the peak FRF value in the most flexible mode. Therefore, the real and imaginary parts of the FRFs of the bare boring bar and the boring bar with dampers were calculated and displayed in Figure 6.1 and Figure 6.2. As shown in Figure 6.1, there was a 7.45-fold reduction in the real part of the FRF.

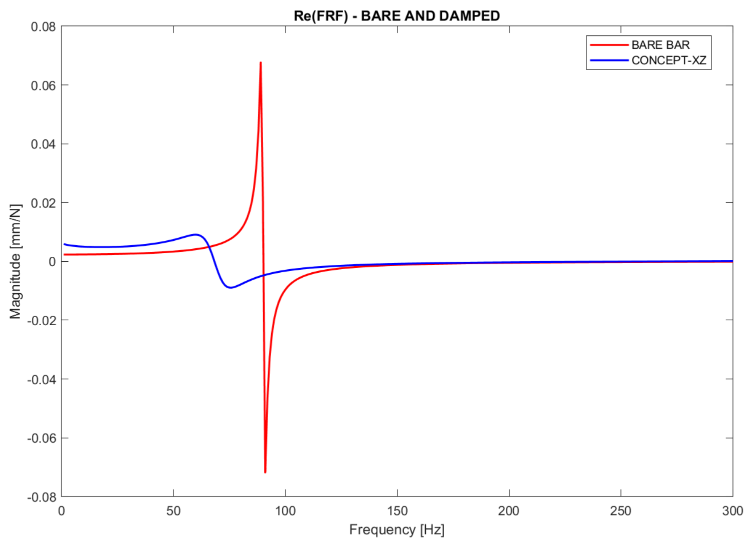

Figure 6.1: FRF - Real Part

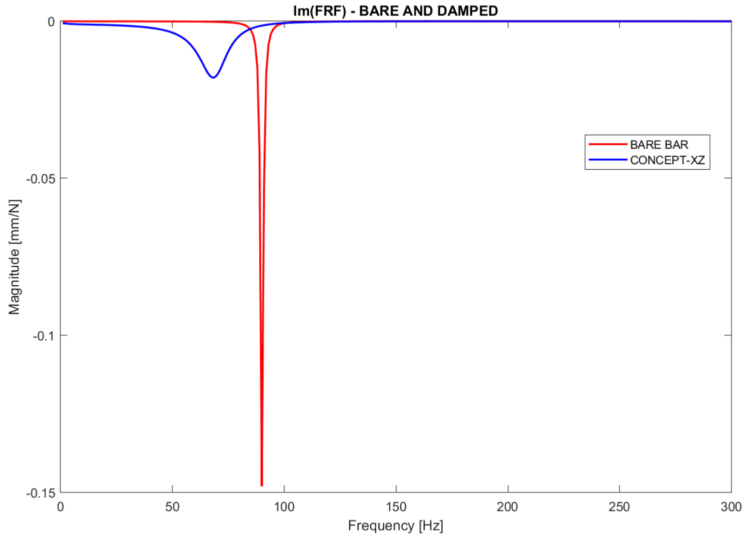

Figure 6.2: FRF - İmaginary Part

The study involved calculating the real and virtual parts of the FRFs for three directions, for both damped and bare boring bars. The stability lobe diagrams were obtained using CutPro software and are presented in Figure 6.3. The diagrams clearly show that the limit depth of cut increased from 1.4 mm to 2.1 mm after the application of the viscoelastic damper. This demonstrates a 1.5 times increase in productivity.

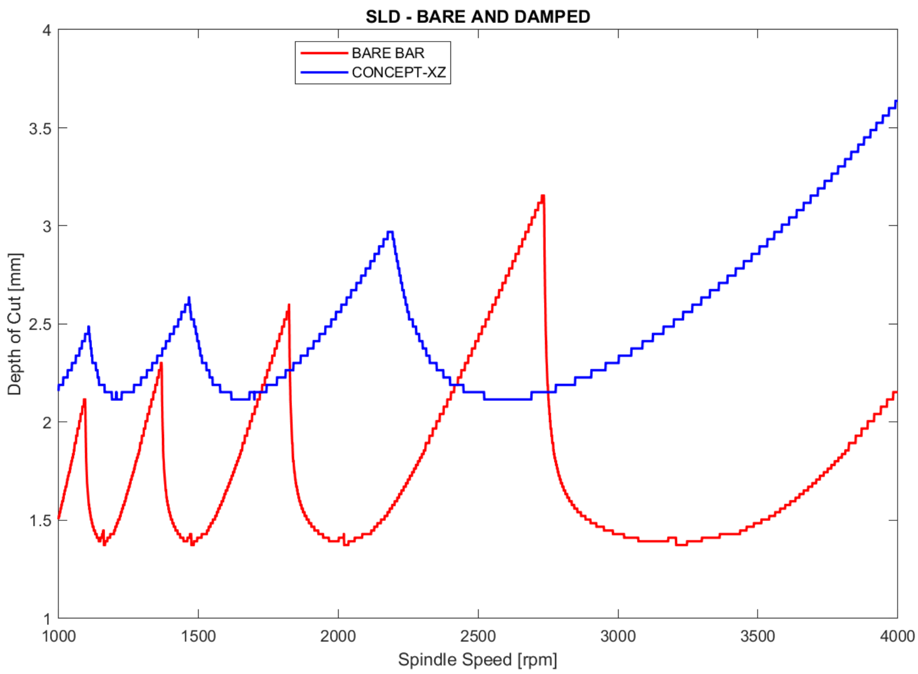

Figure 6.3: SLD of Bare and CONCEPT-XZ Damped Bar

6.2 Comparision Against Other Passive Damping Studies

In this thesis, viscoelastic dampers were designed and applied to dampen the vibrations of boring bars. Among the dampers analyzed and optimized for different usage scenarios, the design obtained in Scenario-2, which minimizes the amplitude at the FRF peak, proved to be the most effective. In this design, the vibration amplitude could be reduced by 8.21 times compared to the undamped bar, while for the other two scenarios, the reduction fold is around 5.6. The visual representation of the best design is shown in Figure 6.4, and the design parameters are presented in Table 6.1. The results obtained have been compared with other studies in the literature, as illustrated in Table 6.2. The results show that viscoelastic damper integration to boring bars is a suitable concept that is novel. It has more damping compared with other techniques except designs with TMD. Also, if a tuning of TMD is not perfect, there is a close gap between our design and designs with TMDs. Unlike TMD, viscoelastic dampers can be implemented simply and with a lower cost.

Table 6.1: Damper Properties of Best Design

Property	Value
Bar Diameter	40mm
Bar Length	560mm
Step Diameter	30mm
Maximum Link Diameter	45mm
Link Length	300mm
VEM Thickness	0.24mm

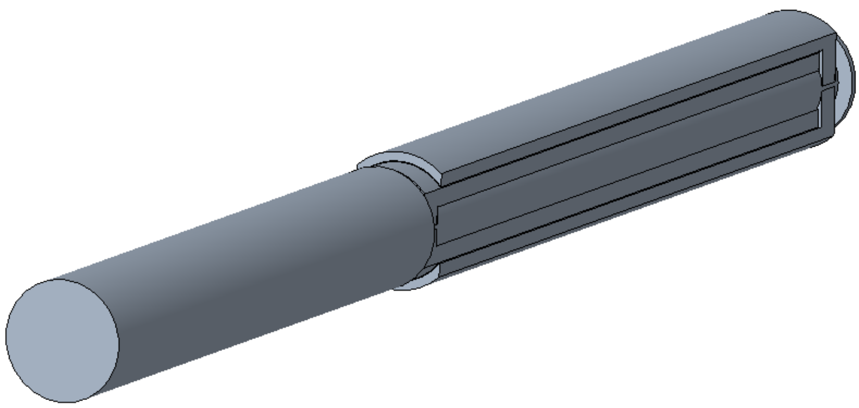

Figure 6.4: Best Design

Table 6.2: Performance of Different Designs

Author	**Damping Technique**	**Red. Fold of Vibration Amplitude**
Zyl [15]	TMD	63.1
Thomas [16]	TMD	22.5
Thomas [16]	PID	6.9
Liu [13]	TMD	2.5
Bansal [14]	TMD	10
Chockalingam [17]	PID	2.2
Hayati [18]	Friction	1.4
Yiğit [23]	Piezoelectric Shunt	3.25

CHAPTER 7

CONCLUSION

In this thesis, the aim was to reduce the vibrations experienced in boring bars. To achieve this, a novel approach that had not been previously explored in literature was introduced. The method involved the use of viscoelastic dampers to improve the stability limits of boring bars and mitigate the vibrations. The study involved modeling and validating viscoelastic materials using FEM. The modeling and validation process was detailed and comprehensive, ensuring that the design of viscoelastic damper integrations for boring bars was optimized. This optimization process was conducted with the goal of reducing the FRF amplitude at the tool tip.

Different types of viscoelastic dampers are designed and analyzed in the study. Firstly, for proper viscoelastic material selection, temperature distribution on boring bar during operation is researched. According to the studies in the literature, it was decided that the choice of a viscoelastic material with high damping coefficients at room temperature was appropriate. As a result of this decision, 3M ISD-112 and 3M 467MP were selected as viscoelastic materials due to their easy availability. Then, five different concept designs were created, three of which were shear configuration. These shear configurations are intended to force the viscoelastic material into shear deformation, while the other two configurations are intended for bending and tension-compression. Comparisons between conceptual designs showed that better damping performance could be achieved with shear configurations. After these comparisons, two most promising concepts which are named as CONCEPT-YZ and CONCEPT-XZ are selected . These two shear configuration dampers are optimized for three different scenarios. Optimization studies show that design which gives best performance is CONCEPT-XZ dampers integrated boring bar for Scenario-2.

In this design, the vibration amplitude could be reduced by 8.21 times compared to the undamped bar, while for the other two scenarios, the reduction fold is around 5.6. This improvement is achieved through a novel passive method, and it surpasses many other passive techniques. The most promising design also manufactured, and simulation results are validated experimentally.

The study concluded by successfully achieving the goal of creating a cost-effective and highly vibration-damped boring bar configuration. The results of this study can be used as a reference point for future research in this field and can be used to improve the design of boring bars to reduce vibrations and improve stability limits.

Future studies can be carried out on increasing the rigidity of rigid links connected by viscoelastic materials. This improvement will both increase the amount of strain energy stored on the viscoelastic material and improve the damping performance. It is also expected to prevent the natural frequency drop by contributing to the overall system stiffness. In addition, studies on different link designs and the application of the viscoelastic damper concept to different machining tools can be carried out in the future.

REFERENCES

[1] T. L. Schmitz and K. S. Smith, *Machining Dynamics Frequency Response to Improved Productivity*. Springer, 2019.

[2] K. Sørby, "Development and optimization of vibration-damped tool holders for high length-to-diameter boring operations," *High-speed machining*, 2017.

[3] R. Lakes, *Viscoelastic Materials*. Cambridge University Press, 2009.

[4] A. D. Nashif, D. I. G. Jones, and J. P. Henderson, *Vibration Damping*. Wiley, 1985.

[5] D. I. G. Jones, *Handbook of Viscoelastic Vibration Damping*. Wiley, 2001.

[6] 3M Company, "3m viscoelastic damping polymer 112 series," tech. rep., 2017.

[7] 3M Company, "467mp material data card.".

[8] A. A. Sonief, A. N. Fauzan, F. Azlan, and M. A. Bashori, "Chatter vibration comparison between normal helix angle and variable helix angle in end milling process based on spectrum analysis," *Jurnal Rekayasa Mesin*, 2020.

[9] C. Huang, W.-A. Yang, X. Cai, L. Weichao, and Y. You, "An efficient third-order full-discretization method for prediction of regenerative chatter stability in milling," *Shock and Vibration*, 2020.

[10] C. V. Biju and M. S. Shunmugam, "Investigation into effect of particle impact damping (pid) on surface topography in boring operation," *The International Journal of Advanced Manufacturing Technology*, 2014.

[11] H. Takeyama, N. Iijima, N. Nishiwaki, and K. Komoto, "Improvement of dynamic rigidity of tool holder by applying high-damping material," *CIRP Annals*, 1984.

[12] M. Miguélez, L. Rubio, J. Loya, and J. Fernández-Sáez, "Improvement of chatter stability in boring operations with passive vibration absorbers," *International Journal of Mechanical Sciences*, 2010.

[13] X. Liu, Q. Liu, S. Wu, L. Liu, and H. Gao, "Research on the performance of damping boring bar with a variable stiffness dynamic vibration absorber," *The International Journal of Advanced Manufacturing Technology*, 2016.

[14] A. Bansal and M. Law, "A receptance coupling approach to optimally tune and place absorbers on boring bars for chatter suppression," *Procedia CIRP*, 2018. 8th CIRP Conference on High Performance Cutting (HPC 2018).

[15] D. van Zyl, Y. Altintas, and D. Ostling, "Parametric design of boring bars with adaptive tuned mass dampers," *CIRP Journal of Manufacturing Science and Technology*, 2022.

[16] W. Thomas, J. Peterka, T. Szabó, M. V. Albuquerque, R. Pederiva, and L. P. Kiss, "Analytical and experimental investigation of the dynamic stability in passive damper boring bars," *Procedia CIRP*, 2023. 19th CIRP Conference on Modeling of Machining Operations.

[17] S. Chockalingam, U. Natarajan, and A. G. Cyri, "Damping investigation in boring bar using hybrid copper-zinc particles," *Journal of Vibration and Control*, 2017.

[18] S. Hayati, M. Shahrokhi, and A. Hedayati, "Development of a frictionally damped boring bar for chatter suppression in boring process," *The International Journal of Advanced Manufacturing Technology*, 2021.

[19] Z. Yuhuan, R. Yongsheng, T. jishuang, and M. jingmin, "Chatter stability of the constrained layer damping composite boring bar in cutting process," *Journal of Vibration and Control*, 2019.

[20] V. V. Krishna, S. Saravanamurugan, P. S. Kishore, K. Yedhu, G. K. Iswar, and A. Shanmughasundaram, "Vibration control in boring process using a constrained viscoelastic layer damper," *IOP Conference Series Materials Science and Engineering*, 2021.

[21] Q. Song, J. Shi, Z. Liu, Y. Wan, and F. Xia, “Boring bar with constrained layer damper for improving process stability,” *The International Journal of Advanced Manufacturing Technology*, 2015.

[22] G. S. Venter, L. M. do Paraizo Silva, M. B. Carneiro, and M. M. da Silva, “Passive and active strategies using embedded piezoelectric layers to improve the stability limit in turning/boring operations,” *The International Journal of Advanced Manufacturing Technology*, 2017.

[23] U. Yigit, E. Cigeroglu, and E. Budak, “Chatter reduction in boring process by using piezoelectric shunt damping with experimental verification,” *Mechanical Systems and Signal Processing*, 2017.

[24] D. J. Glaser and C. L. Nachtigal, “Development of a hydraulic chambered, actively controlled boring bar,” *ASME J. Manuf. Sci. Eng.*, 1979.

[25] S. G. Tewani, K. E. Rouch, and B. L. Walcott, “A study of cutting process stability of a boring bar with active dynamic absorber,” *International Journal of Machine Tools and Manufacture*, 1995.

[26] B.-K. Min, G. O’Neal, Y. Koren, and Z. Pasek, “A smart boring tool for process control,” *Mechatronics*, 2002.

[27] W. Chiu, F. Lam, and D. Gao, “An overhung boring bar servo system for on-line correction of machining errors,” *Journal of Materials Processing Technology*, 2002.

[28] H. Tanaka, F. Obata, T. Matsubara, and H. Mizumoto, “Active chatter suppression of slender boring bar using piezoelectric actuators,” *JSME international journal. Ser. C, Dynamics, control, robotics, design and manufacturing*, 1994.

[29] N. Grossi, L. Croppi, A. Scippa, and G. Campatelli, “A dedicated design strategy for active boring bar,” *Applied Sciences*, 2019.

[30] M. Wang and R. Fei, “Chatter suppression based on nonlinear vibration characteristic of electrorheological fluids,” *International Journal of Machine Tools Manufacture*, 1999.

[31] D. Mei, T. Kong, A. J. Shih, and Z. Chen, “Magnetorheological fluid-controlled boring bar for chatter suppression,” *Journal of Materials Processing Technology*, 2009.

[32] J. Niu, J. Hou, Y. Shen, and S. Yang, “Dynamic analysis and vibration control of nonlinear boring bar with fractional-order model of magnetorheological fluid,” *International Journal of Non-Linear Mechanics*, 2020.

[33] F. Chen, M. Hanifzadegan, Y. Altintas, and X. Lu, “Active damping of boring bar vibration with a magnetic actuator,” *IEEE/ASME Transactions on Mechatronics*, 2015.

[34] A. A. Alhasa, M. Vafaei, S. C. Ali, and T. W. Jian, “Viscoelastic damper for vibration mitigation of footbridges,” *IOP Conf. Ser.: Earth Environ. Sci.*, 2023.

[35] B. Samali and K. C. S. Kwok, “Viscoelastic damper for vibration mitigation of footbridges,” *Engineering Structures*, 1995.

[36] M. S. Eskandar, Nasab, Y.-Q. Guo, and J. Kim, “Seismic retrofit of a soft first-story building using viscoelastic dampers considering inherent uncertainties,” *Journal of Building Engineering*, 2022.

[37] Y. Chen, C. Chen, Q. Ma, H. Jiang, and Z. Wan, “Study on mechanical properties of high damping viscoelastic dampers,” *Advances in Structural Engineering*, 2019.

[38] Çağrı Koçan, “Structural vibration control in wind turbines,” 2019.

[39] A. Kus, Y. Isik, M. Cakir, and S. Coşkun, “Thermocouple and infrared sensor-based measurement of temperature distribution in metal cutting,” *Sensors*, 2015.

[40] B. Paramasivam, “Investigation on the effects of damping over the temperature distribution on internal turning bar using infrared fusion thermal imager analysis via smartview software,” *Measurement*, 2020.

[41] *ANSYS Mechanical APDL Material Reference*.

[42] J. Soovere and M. Drake, “Aerospace structures technology damping design guide volume iii - damping material data,” tech. rep., AFWAL-TR-84-3089, 1985.

[43] B. Çavuş, “Investigation of novel geometrical design concepts for damping treatments,” 2022.

[44] K. O. Eyyüpoğlu, “Development of a novel surface damping treatment,” 2016.

[45] D. van Zyl, *Parametric design of boring bars with adaptive tuned mass dampers*. PhD thesis, University of British Columbia, 2021.

APPENDIX A

MATLAB Scripts to derive frequency-dependent material properties for the ISD-112 material: "

```
clear all;
close all;
clc;

A=[290,210,360,0.5956e 1,0.1474,0.9725e 2];
B=[0.4307,1200,0.1543e+7,0.6847,3.241,0.18];
T=303.15;

alpha T=alpha T(A,B,T);
j=0;
for i=0:1:300
    j=j+1;
    freq(j)=i;
    [G re(j),G im(j),etha(j)]=Gvem(B,i alpha T);
end

o = fopen( vemprop.txt , w );
for i=1:1:j
fprintf(o, nTBPT,, .2f, .2f, .2f,, , ...
[freq(i),G re(i),G im(i)] );
end
```

```
function alphaT=alphaT(A,B,T)
TZ=A(1);
TL=A(2);
TH=A(3);
SAZ=A(4);
SAL=A(5);
SAH=A(6);

CA=(1/TL 1/TZ) 2;
CB=1/TL 1/TZ;
CC=SAL SAZ;
DA=(1/TH 1/TZ) 2;
DB=1/TH 1/TZ;
DC=SAH SAZ;
DE=DB CA CB DA;
a=(DB CC CB DC)/DE;
b=(CA DC DA CC)/DE;

alphaT=10 (a (1/T 1/TZ) 2+b (1/T 1/TZ)+SAZ);
end
```

```
function [Gre,Gim,etha]=Gvem(B,fR)

Ge=B(1);
G1=B(2);
f1=B(3);
beta1=B(4);
c1=B(5);
alpha1=B(6);

G=Ge+G1/(1+c1 (1i fR/f1) ( alpha1) ...
+(1i fR/f1) ( beta1));
Gre=real(G);
```

```
Gim=imag(G);
etha=Gim/Gre;
end
```